ARTICLES

Electromagnetic production of associated strangeness

J. C. David,[1,2] C. Fayard,[1] G. H. Lamot,[1] and B. Saghai[2]
[1]*Institut de Physique Nucléaire de Lyon, Institut National de Physique Nucléaire et de Physique des Particules, CNRS, Université Claude Bernard, F-69622 Villeurbanne Cedex, France*
[2] *Service de Physique Nucléaire, Commissariat à l'Enérgie Atomique, Direction des Sciences de la Matière, DAPNIA, Centre d'Etudes de Saclay, F-91191 Gif-sur-Yvette, France*
(Received 2 November 1995)

A formalism, based on an isobaric approach using Feynman diagrammatic techniques, which includes the nucleonic (spin $\leqslant 5/2$), hyperonic (spin 1/2), and kaonic resonances, is developed. Using this formalism, a thorough investigation of the following electromagnetic strangeness processes, for which experimental results are available, is performed: $\gamma p \to K^+\Lambda$, $K^+\Sigma^0$, $K^0\Sigma^+$, for $E_\gamma^{\rm lab} \leqslant$ 2.1 GeV, $ep \to e'K^+\Lambda$, $e'K^+\Sigma^0$, and $K^-p \to \gamma\Lambda, \gamma\Sigma^0$. A reaction mechanism, describing well enough the data, is found to include a reasonable number of baryonic resonances among a very large number of potential candidates. The extracted main kaon-hyperon-nucleon coupling constants are in good agreement with values predicted using SU(3) symmetry. The main findings of this model are compared with the results of other recent phenomenological studies. Predictions for the upcoming photoproduction polarization and electroproduction observables are presented, and their sensitivity to the phenomenological models ingredients are emphasized. [S0556-2813(96)01606-8]

PACS number(s): 25.20.Lj, 25.30.Rw, 13.88.+e, 13.60.−r

I. INTRODUCTION

The investigation of strangeness production from a proton, using real [1–3] or virtual [1,3,4] photons, started in the late 50s, but a comprehensive description of the underlying reaction mechanism is still not available. This uncomfortable situation, compared to that of pion photoproduction, which is dominated basically by one nucleonic resonance, might be attributed to the more complex role played by the strange quark versus that engendered by *u* and *d* quarks. The introduction of this additional degree of freedom leads to the fact that, even close to the threshold, *a priori* a rather copious number of nucleonic and hyperonic resonances may intervene in the process. In addition, the lack of knowledge of several relevant coupling constants adds to the complexity of the phenomenological investigations in this field. In nourishing the hope of evolving towards a subnucleonic description of, at least, the elementary reactions, efforts to understand the highlights and shortcomings of approaches based on baryonic and mesonic degrees of freedom are of special interest. In this context, such formalisms are called upon to show the domain of validity of such interpretations as clearly as possible and to eventually offer evidence for the crucial need for descriptions which introduce quark-gluon constituents of the hadrons *explicitly*, where approaches based on simple quark models are being initiated [5,6]. This transition frontier in the strangeness realm is expected to become clear due to the theoretical and experimental efforts underway.

Actually, the new generation of electron accelerators and associated detectors have motivated several proposals at the Continuous Electron Beam Accelerator Facility (CEBAF) [7], ELectron Stretcher Accelerator (ELSA) [8], and European Synchrotron Radiation Facility (ESRF) [9].

The photoproduction reactions that are being, or will be, studied in the near future at all of the above three laboratories, will focus on the following reactions:

$$\gamma + p \to K^+ + \Lambda, \tag{1.1}$$

$$\gamma + p \to K^+ + \Sigma^0, \tag{1.2}$$

$$\gamma + p \to K^0 + \Sigma^+. \tag{1.3}$$

Reaction (1.1) is by far the one most studied, both theoretically (see, e.g., Refs. [1–3]) and experimentally [8,10], including polarization observables measurements [11,12]; although, a large part of the existing data base suffers from inconsistencies [2] within the reported accuracies. There are less extensive investigations [3,8,10,13] of the reaction (1.2). Finally, the third process (1.3) has up to now received very little consideration [5,14], probably because of experimental difficulties [15] in identifying the final state particles.

The high duty cycle electron beam and the associated detectors at CEBAF also allow envisioning high quality electroproduction data [7] for the elementary reactions

$$e + p \to e' + K^+ + \Lambda, \tag{1.4}$$

$$e + p \to e' + K^+ + \Sigma^0. \tag{1.5}$$

Here, the virtual photon has besides the transverse component a longitudinal part and offers the possibility of varying independently the energy and momentum transfers. In this respect, the electrons are a finer probe for the strangeness realm. At the present time, the data [16] in this field are scarce, and they have been used only in two phenomenological analysis [3,17].

Although each of the above reactions is interesting by itself, a desirable step by step investigation necessitates first the understanding of the elementary photoproduction reactions. An extension to the electroproduction processes with enough confidence in the reaction mechanism constitutes the next stage. Afterwards, we can take benefit of the much cleaner electromagnetic probes, compared to hadronic ones, to study the strangeness in composite hadronic systems, especially the hypernuclei physics [18].

A very attractive feature of the above reactions comes from their self-analyzing character which allows measuring directly the polarization of the outgoing hyperon. Besides, both at CEBAF and ESRF, polarized beams will be available, and polarized targets are also being developed. Therefore, the single and double polarization measurements will be achievable as the first generation of experiments with the shortly upcoming facilities. Such data will of course provide strong constraints on the phenomenological formalisms.

In such formalisms, the amplitudes of the strangeness photoproduction can be related by crossing symmetry [19] to those of $K^- p$ radiative capture processes

$$K^- + p \rightarrow \gamma + \Lambda, \tag{1.6}$$

$$K^- + p \rightarrow \gamma + \Sigma^0. \tag{1.7}$$

Here, the relevant quantity is the branching ratio defined as

$$R_{\gamma Y} = \frac{\Gamma(K^- p \rightarrow \gamma Y)}{\Gamma(K^- p \rightarrow \text{all})}, \tag{1.8}$$

with $Y \equiv \Lambda, \Sigma^0$. The only reliable data [20] on the branching ratios have been measured at Brookhaven, with stopped kaons.

While the threshold energies for the reactions (1.1) and (1.2) are $E_\gamma^{\text{lab}} = 0.911$ and 1.045 GeV, respectively, the energy of the outgoing γ in the radiative capture processes (1.6) and (1.7) is only about 0.3 GeV. This ''kinematical'' fact has serious implications on the phenomenological models. Besides, as we will also see later, even within a given reaction the sensitivity, and so the selectivity of different observables to the ingredients of the models show a large variety. Hence, the use of a *single* formalism to understand *simultaneously* all the above seven reactions, including polarization observables, offers a powerful mean in disentangling the underlying reaction mechanism.

The most extensive theoretical investigations in this field, between threshold and roughly $E_\gamma^{\text{lab}} = 2$ GeV, are based on isobaric approaches, following the pioneer works by Thom [21] and Renard and Renard [22,23], revived in early 80s by Hsiao and Cotanch [24], and Adelseck, Bennhold, and Wright [25]. All these formalisms use the Feynman diagrammatic techniques. A comprehensive discussion on both theoretical and experimental studies prior to 1990 can be found in Ref. [2]. Since then, three major models, based on isobaric approaches, have been published. The first one by Adelseck-Saghai [2] focuses on the first reaction (1.1) for $E_\gamma^{\text{lab}} \leqslant 1.5$ GeV. The second one, by Williams, Ji, and Cotanch [3], improving their previous studies [26], investigates all the above reactions (1.1)–(1.7) except the $\gamma + p \rightarrow K^0 + \Sigma^+$ channel, and extends the energy range to $E_\gamma^{\text{lab}} \leqslant 2.1$ GeV. Finally, the most recent model, by Mart, Bennhold, and Hyde-Wright [14], is dedicated to the $K\Sigma$ photoproduction channels with a special emphasis on the charged Σ production in the same energy range as Williams *et al.* [3].

The goals of the present work are to obtain a *single* model for *all* the reactions (1.1)–(1.7), and to cure the shortcomings of the above models without losing their findings, and in some cases improving them. The requirements [27] for such a model are then (i) reproduce with a reasonable χ^2 *all* the existing data for *all* of the seven reactions (1.1)–(1.7) in the *whole* energy range where experimental results are available, (ii) satisfy the SU(3)-symmetry constraints on the two main coupling constants, (iii) *predict* correctly at least the experimental results for one observable purposely omitted in the fitted data base, (iv) obtain a rather simple reaction mechanism.

To achieve these aims, the main novelty of the present formalism is, besides spin-1/2 baryonic resonances, the inclusion of spin-3/2 and spin-5/2 nucleonic resonances. Using this formalism, we have obtained a model in line with the requirements put forward in the previous paragraph.

The paper is structured as follows. In the second section, the formalism is outlined. In the third section the fitting procedure and the model ingredients are discussed. The fourth section is devoted to the results, comparisons with the data, as well as with other recent models. In the same section, we also produce predictions for some observables planned to be measured in the near future at CEBAF, ELSA, and ESRF, with an strong emphasis on the photoproduction polarization observables and on the electroproduction reactions. The summary and conclusions are presented in the last section.

II. FORMALISM

In this section, we describe the theoretical framework used in our approach. We simply recall the main lines of the model, and refer the reader to the literature on the subject for more details, especially Refs. [2,3,17,25,28]. For clarity, the expressions of the invariant amplitudes, which are the key quantities of the model, are reported in separate appendices.

A. Isobaric model

We investigate the photo- and electroproduction of kaons on the proton at center of mass energies $\leqslant 2.5$ GeV, and the associated radiative capture branching ratios at threshold. These reactions are described within the framework of an isobaric model, where the amplitudes are expressed as Feynman diagrams. In what follows, we consider the photo- and electroproduction amplitudes associated with the $K^+\Lambda$, $K^+\Sigma^0$, and $K^0\Sigma^+$ channels (only the photoproduction is considered in this last channel[1]). The amplitudes for the radiative capture can easily be obtained *via* crossing symmetry.

We use first-order perturbation theory, where each diagram corresponds to the exchange of *one* particle or resonance (tree approximation). The corresponding diagrams are the so-called extended Born terms for the exchange of the

[1]To obtain the electroproduction channel for $K^0\Sigma^+$, one needs to take into account the Fubini-Nambu-Wataghin [29] term, not discussed here.

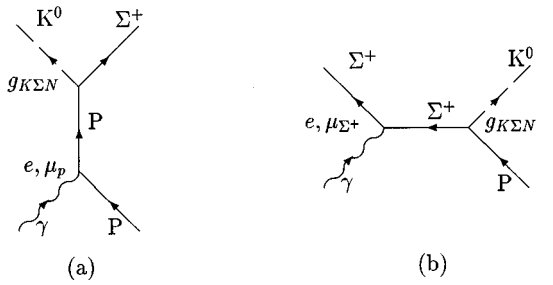

FIG. 1. Extended Born terms for the reaction $\gamma p \to K^0 \Sigma^+$.

proton (p), kaon (K), and hyperon (Y), and the resonant terms for the exchange of the N^*, K^*, and Y^* resonances. In the reactions where a Σ is produced, we also include the Δ resonances as permitted by isospin conservation. As an example, we show in Fig. 1 the Born terms for the reaction $\gamma p \to K^0 \Sigma^+$. The relevant Born terms for $K^+ Y$ channels can be found in the literature (see, e.g., Ref. [3]).

The resonances that can be handled in our approach are the spin $\leqslant 5/2$ ones in the s channel, the spin-1/2 resonances in the u channel, and the $K^*(892)$ and $K1(1270)$ resonances in the t channel (the corresponding diagrams are given in Fig. 2). All of them have their mass $\leqslant 2$ GeV. In Table I, we summarize the characteristics (and notation used) for all exchanged particles and resonances considered in the present work.

Each Feynman diagram leads to a gauge invariant amplitude, except for the extended Born terms corresponding to the exchange of a charged baryon (Dirac coupling $e\gamma^\mu$). So, in the case of K^+ photoproduction associated with the Λ or Σ^0, it is necessary to include the K^+ exchange Born term in order to restore gauge invariance which is broken by the proton exchange, while in the K^0 production associated with the Σ^+, the proton and Σ^+ exchanges together ensure gauge invariance.

The Lorentz invariant matrix element for electroproduction is written as

$$M_{fi} = i\overline{U_Y}\left(\sum_{j=1}^{6} \mathcal{A}_j \mathcal{M}_j\right) U_p \,. \tag{2.1}$$

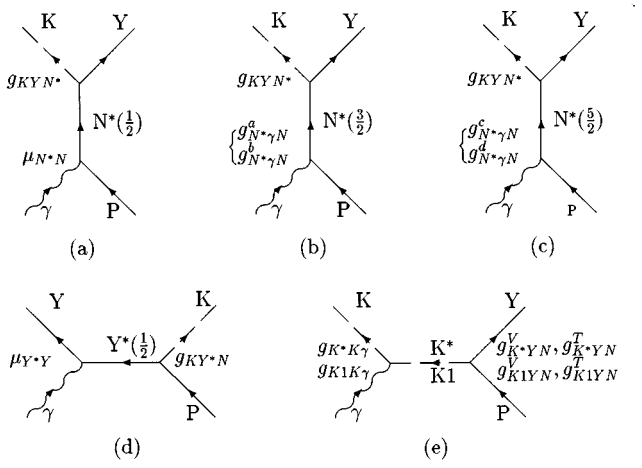

FIG. 2. Resonant terms for the reactions $\gamma p \to KY$, with $(K,Y) \equiv (K^+,\Lambda)$, (K^+,Σ^0), (K^0,Σ^+). The spin of the resonance is given in brackets.

TABLE I. Particles considered in this study. Values (Ref. [54]) for mass and width as used in our calculation are given in the last two columns, respectively.

Notation	Particle	(I)J^π	Mass (MeV)	Width (MeV)
	p	$1/2^+$	938.272	
	K^+	0^-	493.677	
	K^0	0^-	497.672	
	Λ	$1/2^+$	1115.68	
	Σ^0	$1/2^+$	1192.55	
	Σ^+	$1/2^+$	1189.37	
K^{*+}	$K^*(892)^+$	1^-	891.59	49.8
K^{*0}	$K^*(892)°$	1^-	896.1	50.5
$K1$	$K1(1270)$	1^+	1273.0	90.0
$N1$	$N(1440)$	(1) $1/2^+$	1440	350
$N2$	$N(1520)$	(2) $3/2^-$	1520	120
$N3$	$N(1535)$	(0) $1/2^-$	1535	150
$N4$	$N(1650)$	(0) $1/2^-$	1650	150
$N5$	$N(1700)$	(2) $3/2^-$	1700	100
$N6$	$N(1710)$	(1) $1/2^+$	1710	100
$N7$	$N(1720)$	(1) $3/2^+$	1720	150
$N8$	$N(1675)$	(2) $5/2^-$	1680	150
$N9$	$N(1680)$	(3) $5/2^+$	1680	130
$L1$	$\Lambda(1405)$	(0) $1/2^-$	1407	50
$L2$	$\Lambda(1600)$	(1) $1/2^+$	1600	150
$L3$	$\Lambda(1670)$	(0) $1/2^-$	1670	35
$L4$	$\Lambda(1800)$	(0) $1/2^-$	1800	300
$L5$	$\Lambda(1810)$	(1) $1/2^+$	1810	150
$S1$	$\Sigma(1660)$	(1) $1/2^+$	1660	100
$S2$	$\Sigma(1750)$	(0) $1/2^-$	1750	90
$D1$	$\Delta(1620)$	(0) $1/2^-$	1620	150
$D2$	$\Delta(1900)$	(0) $1/2^-$	1900	200
$D3$	$\Delta(1910)$	(1) $1/2^+$	1910	250
$D4$	$\Delta(1232)$	(1) $3/2^+$	1235	131
$D5$	$\Delta(1600)$	(1) $3/2^+$	1600	350
$D6$	$\Delta(1700)$	(2) $3/2^-$	1700	300
$D7$	$\Delta(1920)$	(1) $3/2^+$	1920	200

Here, $\overline{U_Y}$ and U_p are the spinors of the hyperon and proton, respectively, $\mathcal{A}_j$'s are Lorentz invariant scalar functions of the Mandelstam variables, and $\mathcal{M}_j$'s are the usual six gauge invariant matrices for electroproduction [3,17].

Application of the Feynman rules yields the invariant amplitudes $\mathcal{A}_j$. Their expressions are given in Appendix A for the usual extended Born terms, the K^* resonances, and the $J^\pi = \frac{1}{2}^\pm$ nucleonic and hyperonic resonances. Note that in the photoproduction case, only four gauge invariant matrices are needed, and the form factors reduce to the values 0 or 1 (see Sec. II C).

We now give some details concerning the spin $>1/2$ nucleonic resonances.

B. Nucleonic resonances of spin 3/2 and 5/2

As explained in the Introduction, the model of Adelseck-Saghai [2,27] can be considered as a good model at energies up to $E_\gamma \simeq 1.4$ GeV. Since one of the aims of the present work is to extend that model to higher energies where new experimental data will be available in the near future, we

TABLE II. Vertex factors for the spin-3/2 and -5/2 nucleonic resonances. The matrices $\Gamma_+ = i\gamma_5$ and $\Gamma_- = 1$ ensure parity conservation at the electromagnetic and hadronic vertices. The F's are the form factors as defined in Sec. II C. In second column, N^* is the short notation for the corresponding nucleonic resonance considered in first column.

Vertex	Coupling
$N^*\left(\frac{3}{2}^{\pm}\right)p\gamma$	$\left[g^a_{N^*\gamma p}\left(g^{\mu\nu}-\frac{p_\gamma^\nu\gamma^\mu}{\sqrt{s}\pm M_p}\right)+g^b_{N^*\gamma p}\frac{p_p^\mu p_\gamma^\nu - p_\gamma\cdot p_p g^{\mu\nu}}{(\sqrt{s}\pm M_p)^2}\right]\Gamma_\pm F_2^{N^*}$
$KYN^*\left(\frac{3}{2}^{\pm}\right)$	$\frac{g_{KYN^*}}{M_{N^*}}p_Y^\mu\Gamma_\mp$
$N^*\left(\frac{5}{2}^{\pm}\right)p\gamma$	$\left[\frac{g^a_{N^*\gamma p}}{M_{N^*}}\left(g^{\mu\mu'}p_\gamma^{\nu'}-\frac{p_\gamma^{\mu'}p_\gamma^{\nu'}\gamma^\mu}{\sqrt{s}\mp M_p}\right)+\frac{g^b_{N^*\gamma p}}{M_{N^*}}\frac{p_p^\mu p_\gamma^{\mu'}p_\gamma^{\nu'}-p_\gamma\cdot p_p g^{\mu\mu'}p_\gamma^{\nu'}}{(\sqrt{s}\mp M_p)^2}\right]\Gamma_\mp F_2^{N^*}$
$KYN^*\left(\frac{5}{2}^{\pm}\right)$	$\frac{g_{KYN^*}}{M_{N^*}^2}p_Y^\mu p_Y^\nu\Gamma_\pm$

have added spin $>1/2$ nucleonic resonances which may intervene in the reaction mechanism as energy increases.

Nucleonic resonances of spin 3/2 and 5/2 were taken into account in the original photoproduction model developed by Renard and Renard [22,23,30]. However, their expressions for vertices (i.e., the electromagnetic part) and propagators led to scalar amplitudes $\mathcal{A}_j$ as sums of resonant and nonresonant parts. As the latter contributions bring an undesirable behavior as energy increases, Renard and Renard simply discarded them in the fitting procedure. For this reason, we have used the method proposed by Adelseck *et al.* [25] for spin 3/2, and extended it to the spin-5/2 case. As the expressions are rather intricate, we used MAPLE for symbolic mathematical calculations.

1. Spin 3/2

We adopt the prescriptions given in Ref. [25] for the spin-3/2 propagator and vertex. The propagator is obtained from the expression given by Pilkhun [31], with the mass of the resonance appearing in the numerator replaced by the total invariant energy $\sqrt{s}$

$$P^{3/2}_{\mu\nu}=\frac{\not q+\sqrt{s}}{3(s-M^2_{N^*}+iM_{N^*}\Gamma_{N^*})}\times\left[g_{\mu\nu}+\gamma_\nu\gamma_\mu-\frac{2}{s}q_\mu q_\nu-\frac{1}{\sqrt{s}}(\gamma_\mu q_\nu-\gamma_\nu q_\mu)\right]. \tag{2.2}$$

Here $q=p_\gamma+p_p$ and M_{N^*} is the mass of the resonance. The complex term is introduced to take care of the finite width Γ_{N^*} of the unstable particle.[2]

The spin-3/2 vertex factors are constructed in analogy with those of the Δ resonance in pion photoproduction [31], by replacing the mass of the resonance by $\sqrt{s}$, as in the case of the propagator. The resulting expression for the photoproduction is given in Table II. For positive parity, the dot product with the photon vector polarization leads to

$$V^\nu(N^*p\gamma)=i\left[G_1\left(\not\epsilon^\nu-\frac{p_\gamma^\nu\not\epsilon}{\sqrt{s}+M_p}\right)+G_2\frac{1}{(\sqrt{s}+M_p)^2}(\epsilon\cdot p_p p_\gamma^\nu-p_\gamma\cdot p_p\epsilon^\nu)\right]\gamma_5, \tag{2.3}$$

where G_1 and G_2 stand for the usual coupling constants $g^a_{N^*p\gamma}$ and $g^b_{N^*p\gamma}$, respectively.

As stated by Adelseck *et al.* [25], these prescriptions used for the propagator and vertex are necessary in order to ensure gauge invariance of the scattering amplitude. An explicit proof can be found in Ref. [32].

In the case of electroproduction, we make the gauge transformation on the photon vector polarization

$$\epsilon^\mu\rightarrow\epsilon^\mu-\frac{\epsilon\cdot p_\gamma}{p_\gamma^2}p_\gamma^\mu, \tag{2.4}$$

which implies

$$\not\epsilon\rightarrow\not\epsilon-\frac{\epsilon\cdot p_\gamma}{p_\gamma^2}\not p_\gamma. \tag{2.5}$$

Obviously, this transformation only affects the G_1 contribution in Eq. (2.3). Note that the resulting vertex factor must be multiplied by the form factor $F^{N^*}=F_2^p$, the second Dirac form factor of the proton (see next subsection).

The Lorentz invariant matrix element M_{fi} corresponding to the exchange of an $N^*(3/2^+)$ resonance [for example, Fig. 2(b) with $Y=\Lambda$] is then written

$$M_{fi}=\overline{U_\Lambda}V^\mu(K^+\Lambda N^*)P^{3/2}_{\mu\nu}V^\nu(N^*p\gamma)U_p, \tag{2.6}$$

where

[2]In the following, when unambiguous, we use N^* as a short notation for $N^*_{(3/2^\pm)}$ or $N^*_{(5/2^\pm)}$.

$$V^{\mu}(K^{+}\Lambda N^{*}) = \frac{g_{K\Lambda N^{*}}}{M_{N^{*}}} p_{\Lambda}^{\mu}. \tag{2.7}$$

The resulting invariant amplitudes $\mathcal{A}_j$ for photo- and electroproduction are given in Appendix B.

2. Spin 5/2

We take the spin-5/2 propagator and vertex as defined by Renard and Renard [22,30], and modify it according to the Adelseck *et al.* [25] prescription used in the spin-3/2 case. The resulting propagator is

$$P^{5/2}_{\mu\nu,\mu'\nu'} = \frac{\not{q} + \sqrt{s}}{10(s - M^{2}_{N^{*}} + iM_{N^{*}}\Gamma_{N^{*}})} \mathcal{P}^{5/2}_{\mu\nu,\mu'\nu'}. \tag{2.8}$$

The spin-5/2 projection operator is written as

$$\begin{aligned}\mathcal{P}^{5/2}_{\mu\nu,\mu'\nu'} = {} & 5P_{\mu\mu'}P_{\nu\nu'} - 2P_{\mu\nu}P_{\mu'\nu'} + 5P_{\mu\nu'}P_{\nu\mu'} \\ & + P_{\mu\rho}\gamma^{\rho}\gamma^{\sigma}P_{\sigma\mu'}P_{\nu\nu'} + P_{\nu\rho}\gamma^{\rho}\gamma^{\sigma}P_{\sigma\nu'}P_{\mu\mu'} \\ & + P_{\mu\rho}\gamma^{\rho}\gamma^{\sigma}P_{\sigma\nu'}P_{\nu\mu'} + P_{\nu\rho}\gamma^{\rho}\gamma^{\sigma}P_{\sigma\mu'}P_{\mu\nu'},\end{aligned} \tag{2.9}$$

in terms of the spin-1 projection operator

$$P_{\mu\nu} = -g_{\mu\nu} + \frac{1}{s} q_{\mu} q_{\nu}. \tag{2.10}$$

The expanded expression of the propagator can be found in Ref. [30].

The spin-5/2 vertex factor for positive parity is given in Table II. The dot product with the photon polarization gives in the photoproduction case

$$\begin{aligned}V^{\mu'\nu'}(N^{*}p\gamma) = {} & G_1 \left(\epsilon^{\mu'} p_{\gamma}^{\nu'} - \frac{p_{\gamma}^{\mu'} p_{\gamma}^{\nu'} \not{\epsilon}}{\sqrt{s} - M_p} \right) + \frac{G_2}{(\sqrt{s} - M_p)^2} \\ & \times (\epsilon \cdot p_p p_{\gamma}^{\mu'} p_{\gamma}^{\nu'} - p_{\gamma} \cdot p_p \epsilon^{\mu'} p_{\gamma}^{\nu'}),\end{aligned} \tag{2.11}$$

where G_1 and G_2 now stand for $g^{a}_{N^{*}p\gamma}/M_{N^{*}}$ and $g^{b}_{N^{*}p\gamma}/M_{N^{*}}$, respectively.

The evaluation of the invariant amplitudes proceeds along the same lines as in the spin-3/2 case. Note that the $K^{+}\Lambda N^{*}$ vertex is (see Table II)

$$V^{\mu\nu}(K^{+}\Lambda N^{*}) = \frac{g_{K\Lambda N^{*}}}{M^{2}_{N^{*}}} p_{\Lambda}^{\mu} p_{\Lambda}^{\nu} i\gamma_5. \tag{2.12}$$

As a consequence of the complexity of Eqs. (2.9) and (2.11), the calculation is tedious and the resulting expressions very intricate. We give in Appendix C the most compact form we have obtained for the photoproduction amplitudes. The electroproduction amplitudes are much more lengthy, hence we do not report them here.

We end this subsection with a few comments on the off-shell effects. Actually we have used the prescription of Adelseck *et al.* [25] to define the propagator and the vertex of the spin-3/2 (and spin-5/2) nucleonic resonances. This can be considered as an *ad hoc* method aimed to preserve gauge invariance of the amplitudes. In fact, the treatment of an interacting spin-3/2 baryon in the effective Lagrangian theory [33] takes into account the freedom related to the off-shell behavior of the particle (or resonance) at the vertex. The resulting expressions for the propagator and vertex are more complicated and they depend on new free parameters, the so-called ''off-shell parameters.'' A few years ago, the theoretical aspects of this problem were renewed by Benmerrouche *et al.* [34], and application to the theory of pion photoproduction in the $\Delta(1232)$ region was investigated by Davidson *et al.* [35]. Very recently, Benmerrouche *et al.* [36] have demonstrated clearly the importance of off-shell properties of the spin-3/2 nucleonic resonances in the η meson photoproduction in the $N^{*}(1535)$ resonance region.

We are currently investigating these aspects within our model. Preliminary results concerning the photoproduction processes show that off-shell effects in the case of spin-3/2 nucleonic resonances are rather moderate, justifying the use of the Adelseck *et al.* prescription. A detailed analysis will appear in a forthcoming paper [37].

C. Form factors

In electroproduction processes, virtual photons probe the electromagnetic structure of the involved hadrons. This structure is taken into account in phenomenological models by incorporating form factors appropriate to each hadron. In the present work, we have selected some parametrizations proposed in the literature, without trying to readjust the parameters. We now describe briefly the form factors introduced at the relevant vertices.

1. Baryonic form factors

At the γpp vertex, we have to consider the two form factors of the proton; namely, F_1^p and F_2^p, which are related to the electric (G_E^p) and magnetic (G_M^p) form factors

$$F_1^p = \frac{1}{1-\tau}(G_E^p - \tau G_M^p), \quad F_2^p = \frac{1}{\kappa_p(1-\tau)}(G_M^p - G_E^p), \tag{2.13}$$

where $\tau = p_{\gamma}^2/4M^2$ ($p_{\gamma}^2 < 0$), with κ_p the anomalous magnetic moment of the proton.

These form factors have being studied extensively in the literature. We have retained the model developed by Gari and Krümpelmann (hereafter referred to as GK) in Ref. [38] in its most recent version [39] which gives good agreement with available data. The basis of this approach is the extended vector meson dominance (EVMD) model, combining the vector meson dominance (VMD) hypothesis (appropriate at low p_{γ}^2) with the perturbative QCD approach describing the spacelike region. According to GK, the form factors are expressed in terms of isoscalar (is) and isovector (iv) parts as

$$F_1^p = \frac{1}{2}(F_1^{\mathrm{is}} + F_1^{\mathrm{iv}}), \quad F_2^p = \frac{1}{2\kappa_p}(\kappa_{\mathrm{is}} F_2^{\mathrm{is}} + \kappa_{iv} F_2^{\mathrm{iv}}), \tag{2.14}$$

with

$$F_1^{\rm iv}(Q^2)=\frac{g_\rho}{f_\rho}\frac{m_\rho^2}{m_\rho^2+Q^2}F_1^\rho(Q^2)+\left(1-\frac{g_\rho}{f_\rho}\right)F_1^D(Q^2), \tag{2.15a}$$

$$\kappa_{\rm iv}F_2^{\rm iv}(Q^2)=\kappa_\rho\frac{g_\rho}{f_\rho}\frac{m_\rho^2}{m_\rho^2+Q^2}F_2^\rho(Q^2)+\left(\kappa_{iv}-\kappa_\rho\frac{g_\rho}{f_\rho}\right)F_2^D(Q^2), \tag{2.15b}$$

$$F_1^{\rm is}(Q^2)=\frac{g_\omega}{f_\omega}\frac{m_\omega^2}{m_\omega^2+Q^2}F_1^\omega(Q^2)+\left(1-\frac{g_\omega}{f_\omega}\right)F_1^D(Q^2), \tag{2.15c}$$

$$\kappa_{\rm is}F_2^{\rm is}(Q^2)=\kappa_\omega\frac{g_\omega}{f_\omega}\frac{m_\omega^2}{m_\omega^2+Q^2}F_2^\omega(Q^2)+\left(\kappa_{is}-\kappa_\omega\frac{g_\omega}{f_\omega}\right)F_2^D(Q^2). \tag{2.15d}$$

Here, $Q^2=-p_\gamma^2$, g_ρ and g_ω are the vector meson-nucleon coupling constants, m_ρ^2/f_ρ and m_ω^2/f_ω the couplings of the photon to the vector mesons, and the quantities κ are the magnetic moments. F_i^ρ and F_i^ω denote the meson-nucleon form factors, and F_i^D describes the nucleon nonresonant quark structure, which is responsible for the asymptotic behavior ($Q^2\to\infty$).

In order to have a smooth transition between the low and high Q^2 domains, the following simple form is proposed by GK:

$$F_1^\alpha(Q^2)=\frac{\Lambda_1^2}{\Lambda_1^2+\widetilde{Q}^2}\frac{\Lambda_2^2}{\Lambda_2^2+\widetilde{Q}^2}, \tag{2.16a}$$

$$F_2^\alpha(Q^2)=\left[\frac{\Lambda_1^2}{\Lambda_1^2+\widetilde{Q}^2}\right]^2\frac{\Lambda_2^2}{\Lambda_2^2+\widetilde{Q}^2}, \tag{2.16b}$$

with $\alpha=\rho,\omega,D$, and

$$\widetilde{Q}^2=Q^2\ln\left(\frac{\Lambda_2^2+Q^2}{\Lambda_{\rm QCD}^2}\right)\Big/\ln\left(\frac{\Lambda_2^2}{\Lambda_{\rm QCD}^2}\right). \tag{2.17}$$

The values of the parameters obtained by GK [39] are reported in Table III.

At the $Y\Lambda\gamma$, $Y\Sigma^0\gamma$ vertices ($Y=\Lambda,\Sigma^0$), we have used the two form factors of the neutron, F_1^n and F_2^n. According to GK, these quantities are expressed in a form similar to the proton ones. So we have

TABLE III. Parameters for the nucleonic electromagnetic form factors obtained by Gari and Krümpelmann Ref. [39]. The Λ's are given in GeV/c.

$\kappa_{\rm iv}$	$\kappa_{\rm is}$	g_ρ/f_ρ	κ_ρ	g_ω/f_ω	κ_ω	$\Lambda_1^{\rho,\omega}$	Λ_1^D	Λ_2	$\Lambda_{\rm QCD}$
3.706	−0.12	0.631	3.3	0.658	0.4	0.863	1.21	2.1	0.33

$$F_1^Y=F_1^n=\frac{1}{2}(F_1^{\rm is}-F_1^{\rm iv}),\quad F_2^Y=F_2^n=\frac{1}{2\kappa_n}(\kappa_{\rm is}F_2^{is}-\kappa_{\rm iv}F_2^{\rm iv}). \tag{2.18}$$

κ_n is the anomalous magnetic moment of the neutron, and the isoscalar and isovector parts are the same as for the proton.

For nucleonic (hyperonic) resonances, we choose the second Dirac form factor of the proton (neutron). Namely, F_2^p is introduced at the $\gamma N^* p$ vertices, and F_2^n at the $Y^*\Lambda\gamma$ and $Y^*\Sigma^0\gamma$ vertices.

2. Kaonic form factors

The form factor of the K^+ has not been studied as extensively as for the nucleon. Moreover, the available data are restricted to the low transfer domain ($Q^2<0.15$ GeV$^2/c^2$), which makes it difficult to choose a model valid in the energy range considered in the present work. We have adopted the vector meson dominance (VMD) model as proposed by Williams *et al.* [3,28]:

$$F_{K^+}(Q^2)=\sum_{v=\rho,\omega,\Phi}\left(\frac{g_v}{f_v}\right)\frac{M_v^2}{M_v^2+Q^2-iM_v\Gamma_v}, \tag{2.19}$$

where M_v and Γ_v are the mass and width of the vector meson, respectively.

The three coupling parameters are determined by the known $\Phi\to K^+K^-$ decay width, plus the two normalization constraints $F_{K^+}(Q^2=0)=1$, $F_{K^0}(Q^2=0)=0$. The values obtained by the authors are $g_\rho/f_\rho=0.5$, $g_\omega/f_\omega=0.17$, $g_\Phi/f_\Phi=0.33$, leading to a K^+ charge radius $\langle r_{K^+}^2\rangle=0.335$ fm^2, in good agreement with the experimental value [40]: 0.34 ± 0.05 fm^2.

We have also considered recent results by Cardarelli *et al.* [41]. The charge form factor of the kaon is evaluated using a relativistic constituent quark model based on the light-front formalism [42]. Two models are proposed, the first one assuming the same charge radius for u, d, and s constituent quarks, namely $\langle r\rangle=$ 0.48 fm, and the second one using $\langle r\rangle=0.48$ fm for the u and d quarks and $\langle r\rangle=$ 0.25 fm for the s quark. Here, we have retained the second model, fitted[3] according to the following form:

$$F_{K^+}(Q^2)=\frac{a}{1+Q^2/\Lambda_1^2}+\frac{1-a}{(1+Q^2/\Lambda_2^2)^2}. \tag{2.20}$$

The best fit was obtained with $a=$ 0.398, $\Lambda_1=$ 0.642 GeV/c, and $\Lambda_2=$ 1.386 GeV/c.

For the K^* and $K1$ kaonic resonances, we have chosen the simplified VMD model used by Adelseck-Wright [17]. A monopole form factor was assumed: $F(Q^2)=(1+Q^2/\Lambda^2)^{-1}$, with Λ_{K^*} and Λ_{K1} adjusted to give the best fit to the electroproduction data. The obtained values are $\Lambda_{K^*}=0.95$ GeV/c, $\Lambda_{K1}=0.55$ GeV/c.

[3]The fit was performed on 30 numerical values of the form factor in the range $Q^2=0$–5 GeV^2, which were kindly communicated to us by Dr. G. Salmé and Dr. S. Simula. The results for the first model have been reported elsewhere [43].

We have also considered the extended VMD model (EVMD) proposed by Williams *et al.* [3,28]. The structure of the form factor is similar to the K^+ case, with the following modifications. In addition to the ρ, ω, and Φ, the exchange of the $\Phi^*(1680)$ meson is included. The ρ and ω coupling constants are the same as above for the kaon form factor. The two remaining parameters, fitted to the electroproduction data, are $g_\Phi/f_\Phi=0.77$, $g_{\Phi*}/f_{\Phi*}=0.63$. Moreover, the direct coupling of the photon to the hadron is taken into account with an extra term $\gamma F_\gamma(Q^2)$, for which a monopole form is chosen: $F_\gamma(Q^2)=(1+Q^2/\Lambda^2)^{-1}$, with $\Lambda=0.8$ GeV/c. The normalization of the form factor to unity at $Q^2=0$ determines the strength: $\gamma=1-\Sigma_v(g_v/f_v)$.

Finally, we recall that in the photoproduction case ($Q^2=0$) the form factors are

$$F_1^p=F_2^p=1,\quad F_1^{\Lambda,\Sigma^0}=0,\quad F_2^{\Lambda,\Sigma^0}=1,$$
$$F^{K,K^*,K1}=1,\quad F^{N^*}=F^{Y^*}=1. \tag{2.21}$$

D. Observables

1. Electroproduction

We obtain an alternative representation of the Lorentz invariant matrix elements M_{fi} by expressing Eq. (2.1) in terms of two-component spinors χ. In the c.m. frame, we have

$$M_{fi}=\left[\frac{E_Y+M_Y}{2M_Y}\right]^{1/2}\left[\frac{E_p+M_p}{2M_p}\right]^{1/2}\langle\chi(Y)|\mathcal{F}|\chi(p)\rangle, \tag{2.22}$$

where

$$\mathcal{F}=\boldsymbol{\sigma}.\hat{\boldsymbol{\varepsilon}}\mathcal{F}_1+i(\boldsymbol{\sigma}.\hat{\mathbf{p}}_K)(\boldsymbol{\sigma}\times\hat{\mathbf{p}}_\gamma.\hat{\boldsymbol{\varepsilon}})\mathcal{F}_2+(\boldsymbol{\sigma}.\hat{\mathbf{p}}_\gamma)(\hat{\mathbf{p}}_K.\hat{\boldsymbol{\varepsilon}})\mathcal{F}_3$$
$$+(\boldsymbol{\sigma}.\hat{\mathbf{p}}_K)(\hat{\mathbf{p}}_K.\hat{\boldsymbol{\varepsilon}})\mathcal{F}_4+(\boldsymbol{\sigma}.\hat{\mathbf{p}}_\gamma)(\hat{\mathbf{p}}_\gamma.\hat{\boldsymbol{\varepsilon}})\mathcal{F}_5$$
$$+(\boldsymbol{\sigma}.\hat{\mathbf{p}}_K)(\hat{\mathbf{p}}_\gamma.\hat{\boldsymbol{\varepsilon}})\mathcal{F}_6. \tag{2.23}$$

The $\mathcal{F}_i$'s are the well-known Chew, Goldberger, Low, and Nambu (CGLN) amplitudes [44].

The electroproduction cross section is obtained as

$$\frac{d\sigma}{d\Omega_K}=d\sigma_U+\varepsilon_L d\sigma_L+\varepsilon d\sigma_P\sin^2\theta\cos2\phi$$
$$+\sqrt{2\varepsilon_L(1+\varepsilon)}d\sigma_I\sin\theta\cos\phi. \tag{2.24}$$

Here, θ is the angle between the outgoing kaon and the virtual photon, and ϕ is the azimuthal angle between the kaon production plane and the electron scattering plane (see Fig. 3). Also ε and ε_L are the transverse and longitudinal polarization parameters, respectively

$$\varepsilon=\left[1-2\frac{|\mathbf{p}_\gamma|^2}{p_\gamma^2}\tan^2\left(\frac{\Psi}{2}\right)\right],\quad \varepsilon_L=-\frac{p_\gamma^2}{p_{\gamma0}^2}\varepsilon, \tag{2.25}$$

with Ψ the angle between the momenta of the incoming and outgoing electrons (see Fig. 3). Moreover, $d\sigma_U$ is the cross section for an unpolarized incident photon beam, and the term containing $d\sigma_P$ is the asymmetry contribution of a transversally polarized beam. The cross section of a longitudinally polarized virtual photon is given by $d\sigma_L$, while $d\sigma_I$ contains the interference effects between the longitudinal and transverse components of the beam. The expressions for the cross section in terms of the CGLN amplitudes as well as the relations between these amplitudes and the $\mathcal{A}_j$'s are summarized in Appendix D.

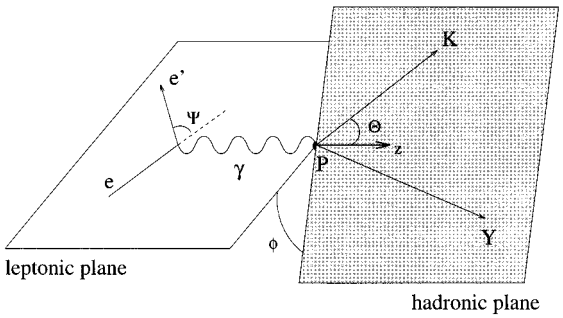

FIG. 3. Leptonic and hadronic planes for kaon electroproduction.

2. Photoproduction

In photoproduction case, $\mathcal{F}$ reduces to the first four terms in Eq. (2.23) since $\hat{\mathbf{p}}_\gamma\cdot\hat{\boldsymbol{\varepsilon}}=0$, and the corresponding $\mathcal{F}_i$'s are simplified as $p_\gamma^2=0$. The resulting differential cross section reduces to the $d\sigma_U$ contribution in Eq. (2.24).

The photoproduction polarization observables are calculated according to the method described in Ref. [2]. We simply recall here the expressions of the polarization observables investigated in this paper.

The single polarization observables are the hyperon polarization asymmetry P, the polarized proton target asymmetry T, and the polarized photon beam asymmetry Σ. They are defined by

$$P=\frac{d\sigma/d\Omega^{(+)}-d\sigma/d\Omega^{(-)}}{d\sigma/d\Omega^{(+)}+d\sigma/d\Omega^{(-)}}, \tag{2.26}$$

$$T=\frac{d\sigma/d\Omega^{(+)}-d\sigma/d\Omega^{(-)}}{d\sigma/d\Omega^{(+)}+d\sigma/d\Omega^{(-)}}, \tag{2.27}$$

$$\Sigma=\frac{d\sigma/d\Omega^{(\perp)}-d\sigma/d\Omega^{(\parallel)}}{d\sigma/d\Omega^{(\perp)}+d\sigma/d\Omega^{(\parallel)}}, \tag{2.28}$$

respectively, where $+$ $(-)$ refers to a hadron polarized parallel (antiparallel) to the $\hat{y}=(\mathbf{p}_\gamma\times\mathbf{p}_K)/(|\mathbf{p}_\gamma\times\mathbf{p}_K|)$ axis, and $\perp$ $(\parallel)$ to a photon linearly polarized perpendicular (parallel) to the reaction plane.

Among the 12 double-polarization observables, we will report in Sec. IV on four of them corresponding to the beam-recoil asymmetries (Table IV). This set is technically the easiest double-polarization observables to be measured. The general expression is

$$X=\frac{d\sigma/d\Omega^{(++)}-d\sigma/d\Omega^{(+-)}}{d\sigma/d\Omega^{(++)}+d\sigma/d\Omega^{(+-)}}$$
$$=\frac{d\sigma/d\Omega^{(--)}-d\sigma/d\Omega^{(-+)}}{d\sigma/d\Omega^{(--)}+d\sigma/d\Omega^{(-+)}}, \tag{2.29}$$

where $+$ $(-)$ denotes a polarization parallel (antiparallel) to the respective quantization axis as specified in Table IV. In

TABLE IV. Photoproduction observables discussed in this paper.

Observable	Polarization [a] of γ	p	Y
(1)$d\sigma$			
Simple polarization			
(2)P			y′
(3)Σ	p		
(4)T		y	
Double polarization beam-recoil			
(5)$C_{x'}$	c		x'
(6)$C_{z'}$	c		z'
(7)$O_{x'}$	t		x'
(8)$O_{z'}$	t		z'

[a]Quantization axes are defined as follows: $\hat{z}=\hat{\boldsymbol{p}}_p, \hat{y}=\boldsymbol{p}_\gamma\times\boldsymbol{p}_K/|\boldsymbol{p}_\gamma\times\boldsymbol{p}_K|, \hat{x}=\hat{y}\times\hat{z}$, $\hat{z}'=\hat{\boldsymbol{p}}_Y, \hat{y}'=\hat{y}, \hat{x}'=\hat{y}'\times\hat{z}'$. p is the linearly polarized photon ($0,\pi/2$ with respect to scattering plane). t is the linearly polarized photon ($\pm\pi/4$ with respect to scattering plane). c is the circularly polarized photon.

the case of a circularly polarized (c) photon beam, $+$ ($-$) is equivalent to the helicity state $+1$ (-1), while in the case of a linearly polarized (t) photon beam, it refers to a state with an angle of 45° (-45°) between the polarization vector and the x axis.

3. Branching ratio

The amplitudes for the kaon photoproduction mechanisms $\gamma p\to K^+Y$, $Y\equiv\Lambda,\Sigma^0$ can be related to radiative kaon capture $K^-p\to\gamma Y$ using crossing symmetry [19]. The only relevant observable for which data are available is the branching ratio for the radiative capture of kaons at rest

$$R_{\gamma Y}=\frac{\Gamma(K^-p\to\gamma Y)}{\Gamma(K^-p\to\text{ all})}. \tag{2.30}$$

Workman and Fearing [45] give expressions for the two disintegration widths Γ in the above equation in terms of the photoproduction transition matrix M_{fi}, assuming the kaon wave function to be a constant

$$\Gamma(K^-p\to\gamma Y)=|\phi_K(0)|^2\frac{M_Y E_\gamma}{4\pi(M_K+M_p)M_K}\sum_{\epsilon,s_p,s_\Lambda}|M_{fi}|^2, \tag{2.31}$$

$$\Gamma(K^-p\to\text{ all})=2\,W_p|\phi_K(0)|^2. \tag{2.32}$$

Here, $W_p=560\pm135$ MeV fm^3 is the imaginary part of the K^-p pseudopotential. The final expression for the branching ratio is

$$R_{\gamma Y}=\frac{M_Y E_\gamma}{8\pi W_p(M_K+M_p)M_K}\frac{1}{2}\sum_{\epsilon,s_p,s_\Lambda}|\widetilde{M}_{fi}|^2, \tag{2.33}$$

with $\widetilde{M}_{fi}$ related to M_{fi} *via* crossing symmetry.

TABLE V. Electromagnetic vertices: magnetic [$\mu_x=\kappa_x(e\hbar/2m_x)$] and Σ^0-Λ transition moments ($\mu_{\Sigma^0\Lambda}=\kappa_{\Sigma^0\Lambda}[e\hbar/(m_{\Sigma^0}+m_\Lambda)]$.

Anomalous magnetic moment	Value [54]
κ_p	1.79
κ_Λ	−0.73
	0.80[a]
κ_{Σ^0}	1.02[b]
	1.21[c]
κ_{Σ^+}	1.85
$\kappa_{\Sigma^0\Lambda}$	1.61

[a]$\kappa_{\Sigma^0}=(\kappa_{\Sigma^+}+\kappa_{\Sigma^-})/2$.
[b]κ_{Σ^0} from quark model, see Ref. [28].
[c]$\kappa_{\Sigma^0}=-(1/2)\kappa_n$.

III. MODEL INPUTS AND FITTING PROCEDURE

In this section, we report on the phenomenological ingredients of our investigations and discuss the procedure that has allowed us to obtain the model presented in this paper, hereafter called SL for Saclay-Lyon.[4] The main features of the other recent isobaric models are also outlined.

A. Propagators and vertices

In the previous section, we described our approach and showed in Figs. 1 and 2 some typical Feynman diagrams. In our effort to determine the reaction mechanism, the main questions are the nature of the propagators, and their strengths. In other words, which resonances are exchanged and what are the corresponding coupling constants? Given that our energy range of interest goes from threshold to $E_\gamma^{\text{lab}}\approx$ 2.1 GeV, the large number of resonances shown in Table I can *a priori* intervene in the reaction mechanism. This table contains all relevant baryonic resonances with masses up to $\approx$ 2 GeV. As explained in the previous section, we take into account all nucleonic resonances with spin $\leqslant$ 5/2, and hyperonic resonances with spin 1/2. The choice of kaonic resonances is based on previous investigations [2,17]. Another difficulty comes from the fact that only a few couplings are known and the other ones have to be determined phenomenologically. The known couplings concern the electromagnetic vertices, and their values as used in this work, are given in Table V.

B. Models

As mentioned in the Introduction, at the present time, the most recent and significant models come from three groups. The first one by Adelseck-Saghai [2,27] (hereafter referred to as AS), focuses on the first reaction (1.1) for $E_\gamma^{\text{lab}}\leqslant$ 1.5 GeV and offers the most comprehensive study of this reaction.

[4]In our code the observables are calculated through a decomposition in terms of the CGLN amplitudes. Given the complexity of the expressions, especially in the case of spin $\geqslant$3/2 resonances, we have cross-checked our numerical results against those obtained with an independent code where the observables are calculated directly using the explicit forms for the vertices and propagators.

TABLE VI. Exchanged resonances and main coupling constants of models by AS [2,27], WJC [3], and MBH [14], with their broken SU(3)-symmetry values [2,46]. The number of free parameters for $K\Lambda$ ($K\Sigma$) channels is shown in the last column.

	s channel	u channel	t channel	$\frac{g_{K\Lambda N}}{\sqrt{4\pi}}$	$\frac{g_{K\Sigma N}}{\sqrt{4\pi}}$	Number of free parameters
AS	$N1$	$L3$	K^*, $K1$	-4.17 ± 0.75	1.18 ± 0.66	8
WJC	$N4$, $N6$, $D1$, $D2$, $D3$	$L1$	K^*, $K1$	-2.38	0.27	9 (12)
MBH	$N4$, $N6$, $D2$, $D3$	—	K^*	0.51	0.13	(8)
SU(3)				-3.7 ± 0.7	1.1 ± 0.2	

The second one by Williams, Ji, and Cotanch [3,28] (hereafter referred to as WJC), investigates all the above reactions (1.1)–(1.7) except the $\gamma p \to K^0\Sigma^+$ channel, and extends the energy range to $E_\gamma^{\rm lab} \leqslant 2.1$ GeV. These authors study the largest number of reactions ever performed and underline the importance of considering the radiative capture channels. Finally the most recent model, by Mart, Bennhold, and Hyde-Wright [14] (hereafter referred to as MBH), is dedicated to $K\Sigma$ photoproduction channels in the same energy range as WJC, with the novelty being a special emphasize on the charged-Σ production channel. In Table VI, we summarize the resonances included in these models, with the conventions introduced in Table I, and the extracted values of the two main coupling constants.

Common to all these models is that they all include *only* spin-1/2 baryonic resonances and determine the unknown coupling constants by fitting the data. These three models contain the same Born terms and t-channel exchanges (except for MBH), but differ in the baryonic resonances in both s and u channels (Table VI) and associated coupling constants. The main features of the AS model are (i) the reaction mechanism is simple, since the model contains only two baryonic resonances, (ii) it reproduces well enough the cross sections for the $K^+\Lambda$ photoproduction channel up to 1.4 GeV, (iii) it predicts correctly all the available polarization asymmetries data (P and T), (iv) the two main coupling constants *come out* in good agreement with their broken SU(3)-symmetry values [2,27,46] and with the values extracted from hadronic sector [47]. The shortcomings of this model are that it overpredicts the (*unfitted*) cross sections above $\approx$ 1.5 GeV (due mainly to the importance of the Born terms [48]) and the radiative capture branching ratio. The WJC model gives rather good agreement with all the fitted data up to $\approx$ 2 GeV, as well as the (*fitted*) branching ratios. However the coupling constants of this model are far from their SU(3) values. Besides, the model does not reproduce [49] the *only* unfitted data set corresponding to the polarized target asymmetry in $\vec{\gamma p} \to K^+\Lambda$ reaction. The last model, MBH, investigates only two of the above reactions, i.e., $\gamma p \to K^+\Sigma^0$, $K^0\Sigma^+$, with couplings much smaller than the SU(3) predictions.

In the next section, we perform a more comprehensive comparison than done in the original papers, between theoretical results from AS, WJC, and MBH and the available data, showing the need for a more sophisticated model reproducing *all* the experimental results simultaneously *and* satisfying the SU(3)-symmetry requirements.

C. Minimization method

To build a new model, we have used all the available data for the seven reactions. Table VII shows the number of data points for each reaction and used in our minimization data base. The minimization was done through least-squares fitting procedure using the MINUIT code [50] from CERN. Because of inconsistencies within the data base, discussed in details in Ref. [2], we have used consistently the total error bars in line with Ref. [2]. The very recent data from ELSA [8] have rather large statistical error bars (roughly $\pm 20\%$) compared to those of the old data [10] ($\pm 4\%$ to $\pm 8\%$). Hence, for the ELSA experimental results we have used only statistical uncertainties in the minimization. Notice that the rather poor accuracies of the ELSA data seem more reliable than the much smaller errors [2] of the old experimental results [10].

The main question here is the ''choice'' of the resonances relevant to the reaction mechanism, given that there are about 30 potential candidates as exchanged particles (Table I). At the present time, there are no unique criteria allowing one to select the relevant intervening resonances. The reason for this uncomfortable situation is that the existing data, coming basically from the $\pi^- p \to K^0\Lambda$ reaction, do not al-

TABLE VII. Number of data points for the reactions considered here and used in our fitting procedure.

Reaction	Number of data points	Ref.
(1) $\gamma p \to K^+\Lambda$	242	[8, 10 [a], 11]
(2) $\gamma p \to K^+\Sigma^0$	195	[8, 10]
(3) $\gamma p \to K^0\Sigma^+$	2	[15]
(4) $ep \to e'K^+\Lambda$	66	[16]
(5) $ep \to e'K^+\Sigma^0$	43	[16]
(6) $K^- p \to \gamma\Lambda$	1	[20]
(7) $K^- p \to \gamma\Sigma^0$	1	[20]

[a]As discussed in Ref. [2].

low extracting the branching ratios for the disintegration of the nucleonic resonances to kaon-hyperon final states. In the latest version of the Particle Data Group (PDG) compilation [51], nonvanishing branching ratios for $N^* \to K\Lambda$ are reported only for resonances $N4-N9$ with large uncertainties. For the $K\Sigma$ final state, no branching ratio information is provided for the 16 nucleonic resonances ($N1-N9$ and $D1-D7$) considered here (Table I). Notice that in the 1990 edition of the PDG [52] the branching ratios reported for $N6 \to K\Sigma$ (2–10 %) and $D7 \to K\Sigma$ ($\sim$ 5%) have been dismissed in the subsequent editions [53,54,51]. Given this situation concerning the relevant branching ratios, [5] in this work we have not favored any of the resonances listed in Table I.

The resonance selection method used to obtain the present SL model is explained in the following. Among the existing models, that by Adelseck-Saghai [2,27] offers an appropriate starting point for the reasons enumerated above. Another appealing feature of this work is that these authors are the only ones to have investigated *all the 4096 possible configurations* with spin-1/2 hadronic resonances and have shown that the model obtained is the *only* satisfactory one. [6] Introducing higher spin resonances increases by a large amount the number of possible configurations, hence an *exhaustive* study becomes prohibitive. Consequently, we chose the AS model as our starting point and moved progressively to more complicated reaction mechanisms. However, thousands of minimizations, with different exchanged resonances content, were performed before obtaining the model presented in this paper.

The first step was thus to extend the Adelseck-Saghai model to higher energies. Actually, the available data cover the energy range from almost threshold to 2.1 GeV. Focusing on the $K^+\Lambda$ photoproduction channel, we introduced the spin-3/2 nucleonic resonances as explained in Sec. II B, and obtained a satisfactory model [56]. As second step [32,57,58] we generalized our approach to study simultaneously all photoproduction *and* the radiative capture reactions. The $K^+\Lambda$ electroproduction reaction was also explored. This was done by adding spin-5/2 nucleonic resonances as well as, for the $K\Sigma$ channels, the isospin-3/2 ones (cf. Sec. II). This latter work was then pursued [43,59,60] with basically an extensive study of the relevant hadronic form factors, leading thus to a complete and simultaneous phenomenological analysis of all seven reactions (1.1)–(1.7). The resulting Saclay-Lyon SL model is presented in this paper. The content of our model, as well as of the other models [2,3,14] mentioned above, are summarized in Tables VIII and IX for $K\Lambda$ and $K\Sigma$ channels, respectively. The reduced χ^2's are 1.73 for all $K\Lambda$ channels, reactions (1.1), (1.4), and (1.6); and 1.04 for all $K\Sigma$ channels, reactions (1.2), (1.3), (1.5), and (1.7). Table X shows the reduced χ^2's for individual channels. The reaction mechanism obtained in this work deserves a few comments, especially with respect to the AS model (Table VIII), which was our starting point.

TABLE VIII. Exchanged particles and coupling constants for $K\Lambda$ channels from models by AS [2], WJC [3], and SL (present work). All the baryonic resonances have spin 1/2, except $N7$ (spin 3/2), and $N8$ (spin 5/2).

Particle	Coupling	AS	WJC	SL
Λ	$g_{K\Lambda N}/\sqrt{4\pi}$	-4.17 ± 0.75	-2.38	-3.16 ± 0.01
Σ	$g_{K\Sigma N}/\sqrt{4\pi}$	1.18 ± 0.66	0.27	0.91 ± 0.10
K^*	$G_V/4\pi$	-0.43 ± 0.07	-0.16	-0.05 ± 0.01
	$G_T/4\pi$	0.20 ± 0.12	0.08	0.16 ± 0.02
$K1$	$G_{V1}/4\pi$	-0.10 ± 0.06	0.02	-0.19 ± 0.01
	$G_{T1}/4\pi$	-1.21 ± 0.33	0.17	-0.35 ± 0.03
$N1$	$G_{N1}/\sqrt{4\pi}$	-1.41 ± 0.60		-0.01 ± 0.12
$N4$	$G_{N4}/\sqrt{4\pi}$		-0.04	
$N6$	$G_{N6}/\sqrt{4\pi}$		-0.06	
$N7$	$G^a_{N7}/4\pi$			-0.04 ± 0.01
	$G^b_{N7}/4\pi$			-0.14 ± 0.04
$N8$	$G^a_{N8}/4\pi$			-0.63 ± 0.10
	$G^b_{N8}/4\pi$			-0.05 ± 0.56
$L1$	$G_{L1}/\sqrt{4\pi}$		-0.07	-0.31 ± 0.06
$L3$	$G_{L3}/\sqrt{4\pi}$	-3.17 ± 0.86		1.18 ± 0.09
$L5$	$G_{L5}/\sqrt{4\pi}$			-1.25 ± 0.20
$S1$	$G_{S1}/\sqrt{4\pi}$			-4.96 ± 0.19

Actually, both AS and SL models satisfy the broken SU(3)-symmetry requirements for the two main coupling constants $g_{K\Lambda N}$ and $g_{K\Sigma N}$. In the AS model these values are obtained by leaving both of them as completely free parameters in the minimization procedure. However, this is not the case for the SL model because of a very large number of possible configurations as explained above. Hence, in the present study these couplings were left free only inside their broken SU(3) values [2,46]; namely, $-4.4 \leqslant g_{K\Lambda N}/\sqrt{4\pi} \leqslant -3.0$ and $+0.8 \leqslant g_{K\Sigma N}/\sqrt{4\pi} \leqslant +1.3$. This also explains the smaller uncertainties in the SL model compared to those of the AS model [27], especially for the first coupling constant. The error bars of the available electromagnetic strangeness production data do not allow extracting $g_{K\Lambda N}$ and $g_{K\Sigma N}$ couplings with accuracies better than $\pm 20\%$ and $\pm 50\%$, respectively [27]. Here, we would like to point out that whether the extracted values for the two main coupling constants from the electromagnetic production of strangeness have to satisfy the SU(3)-symmetry requirements has been a long standing problem in this field and is still a controversial issue (see, for example, Refs. [2,3]).

The present model includes the only (spin-1/2) nucleonic resonance in AS with much smaller strength. In addition, it contains one spin-3/2 and one spin-5/2 nucleonic resonances. The higher spin components in the present model lead to smaller couplings for the *t*-channel exchanges. This confirms the manifestation [61] of the duality hypothesis [62] in the

[5] A comparable situation is encountered in other sectors. For example, recent experimental [55], and theoretical [36] investigations on the reaction $\gamma p \to \eta p$ find a non negligible contribution from $N2$, while no branching ratio for $N2 \to \eta N$ is reported in the PDG [52–54,51].

[6] The two others models, WJC and MBH, were obtained by fixing from the beginning the exchanged particles content of the model (Table VI) in data fitting. Their choices of nucleonic resonances are partly based on the disintegration branching ratios reported in the 1990 edition of the PDG [52] as discussed above.

TABLE IX. Exchanged particles and coupling constants for $K\Sigma$ channels from the models by MBH [14], WJC [3], and SL (present work).

Particle	Coupling	MBH	WJC	SL
Λ	$g_{K\Lambda N}/\sqrt{4\pi}$	0.51	−2.38	−3.23 ± 0.17
Σ	$g_{K\Sigma N}/\sqrt{4\pi}$	0.13	0.27	0.80 ± 0.10
K^*	$G_V/4\pi$	0.05	0.11	0.02 ± 0.01
	$G_T/4\pi$	0.05	−0.14	−0.07 ± 0.02
$K1$	$G_{V1}/4\pi$		−0.13	−0.05 ± 0.01
	$G_{T1}/4\pi$		0.07	0.23 ± 0.04
$N1$	$G_{N1}/\sqrt{4\pi}$			−0.95 ± 0.11
$N4$	$G_{N4}/\sqrt{4\pi}$	0.08	0.09	
$N6$	$G_{N6}/\sqrt{4\pi}$	0.57	0.47	
$N7$	$G^a_{N7}/4\pi$			−0.04 ± 0.02
	$G^b_{N7}/4\pi$			−0.53 ± 0.06
$N8$	$G^a_{N8}/4\pi$			2.02 ± 0.20
	$G^b_{N8}/4\pi$			3.91 ± 0.57
$L1$	$G_{L1}/\sqrt{4\pi}$		0.46	−0.42 ± 0.03
$L3$	$G_{L3}/\sqrt{4\pi}$			−0.10 ± 0.09
$L5$	$G_{L5}/\sqrt{4\pi}$			6.01 ± 0.23
$S1$	$G_{S1}/\sqrt{4\pi}$			−1.72 ± 0.21
$D1$	$G_{D1}/\sqrt{4\pi}$		−0.03	
$D2$	$G_{D2}/\sqrt{4\pi}$	0.07	−0.06	
$D3$	$G_{D3}/\sqrt{4\pi}$	0.30	−0.51	0.43 ± 0.04
$D4$	$G^a_{D4}/4\pi$			−0.47 ± 0.06
	$G^b_{D4}/4\pi$			−1.88 ± 0.14
$D7$	$G^a_{D7}/4\pi$			0.05 ± 0.01
	$G^b_{D7}/4\pi$			0.29 ± 0.04

strangeness field. The applications of this hypothesis to the strangeness sector was performed in the early 70s to the hadronic reactions [63] and, with less conclusive result, to the photoproduction processes [23]. Later, the need for *t*-channel resonance exchanges in the models with only spin-1/2 resonances in the *s* and *u* channels was underlined by Williams *et al.* [3]. Given that our formalism allows including higher spin nucleonic resonances, we investigated the possibility of removing *t*-channel resonances in our model research. This attempt did not allow finding a satisfactory model. Recent progress in a model independent approach [61,64] shows [65] that the present data base for the $K\Lambda$ channels force the *t*-channel resonances in the model discussed here (SL) to mimic spin-7/2 *s*-channel exchanges. Before concluding that such high spin resonances intervene significantly in the reaction mechanisms of the strangeness electromagnetic production and given the amount of work required to include such terms in the formalism, one needs probably more reliable data, as anticipated, from the upcoming facilities.

TABLE X. Partial reduced χ^2 obtained with the present model (SL) for data base reported in Table VII. The number of free parameters for $K\Lambda$ ($K\Sigma$) channels is shown in the last row.

Reaction	χ^2
(1) $\gamma p \to K^+\Lambda$	1.5
(2) $\gamma p \to K^+\Sigma^0$	0.9
(3) $\gamma p \to K^0\Sigma^+$	1.7
(4) $ep \to e'K^+\Lambda$	1.9
(5) $ep \to e'K^+\Sigma^0$	2.7
(6) $K^-p \to \Lambda\gamma$	0.5
(7) $K^-p \to \Sigma^0\gamma$	0.0
Number of free parameters	15(20)

Before ending this section, we discuss the content of the SL model in more detail and the role played by different components of the reaction mechanism so obtained, with the following main goals: (i) are all the exchanged particles indispensable in the reaction mechanism as determined here, (ii) how sensitive are different channels to the ingredients of the model?

This information is summarized in Table XI. The first column gives the relevant reaction, with *all* $K\Lambda$ referring to the reactions (1.1), (1.4), and (1.6), and *all* $K\Sigma$ to the remaining processes (1.2), (1.3), (1.5), and (1.7). The second column refers to the observable for which data are available and have been included in the fitting procedure. The ten subsequent columns have been obtained after removing *one resonance at a time* and *refitting* the complete set of data base. Hence, for example, the third column is generated from an exchanged particles configuration containing *all* those included in the SL model, *except* the $N1$ resonance. This new configuration was then used to fit all the data providing χ^2's for each channel. This procedure leads of course to a new set of couplings for each column.

The $N1$ resonance, because of its tiny coupling in the $K\Lambda$ processes, improves the χ^2 only in the $K\Sigma$ channels. The only spin-3/2 baryonic resonance included in our model ($N7$) is required by the $\gamma p \to K^+\vec{\Lambda}$ and all the electroproduction channels. This resonance plays a crucial role in the K^-p radiative capture, as well as in the charged Σ photoproduction. Besides, we have observed that removing the $N7$ resonance spoils the correct *prediction* for the polarized target asymmetry T in the $\gamma\vec{p} \to K^+\Lambda$ reaction. The last nucleonic resonance $N8$ (spin 5/2) affects not only almost all $K^+\Lambda$ channels, including the recoil Λ-polarization asymmetry, but also improves the χ^2 for the $K^+\Sigma^0$ photoproduction reaction.

The first Λ resonance $L1$ is, as expected, the most important component of the model with respect to radiative capture branching ratios. The next one ($L3$), which is also the only other baryonic resonance in the AS model, shows up in $K\Lambda$ photoproduction and related radiative capture channels. In contrast, the last Λ resonance $L5$, improves the χ^2 for the $K^+\Sigma^0$ photoproduction.

The only retained Σ resonance $S1$ plays a rather minor role, affecting only total cross sections. However, we have found a strong correlation between $L5$ and $S1$. Discarding one of them from the reaction mechanism increases the coupling constant of the kept resonance by roughly a factor of 5. Although there are no indications about the size of these couplings from other sources, such large variations of the couplings, related to resonances with apparently small indi-

TABLE XI. Sensitivity of the χ^2's to the components of the present model (SL). The first two columns give the considered reactions and the fitted observables, respectively. Each of the following columns gives the deterioration of the χ^2 in percentage when the corresponding resonance is switched off. The scale goes from weak to strong as $-<3\%$; $3\%\leqslant *<10\%$; $10\%\leqslant **<20\%$; $20\%\leqslant ***<40\%$; $****\geqslant 40\%$.

Reaction	Observable	$N1$	$N7$	$N8$	$L1$	$L3$	$L5$	$S1$	$D3$	$D4$	$D7$
All $K\Lambda$	All	–	*	*	*	**	–	–			
$\gamma p\rightarrow K^+\Lambda$	$d\sigma$	–	–	*	*	*	–	–			
$\gamma p\rightarrow K^+\vec{\Lambda}$	P	–	***	*	–	***	–	–			
$\gamma p\rightarrow K^+\Lambda$	$\sigma_{\rm tot}$	–	–	–	**	***	–	*			
$ep\rightarrow e'K^+\Lambda$	$d\sigma_{UL}$	–	**	**	–	–	–	–			
$K^-p\rightarrow\gamma\Lambda$	Branching ratio	–	****	**	****	****	–	–			
All $K\Sigma$	All	*	–	–	–	–	–	–	*	**	–
$\gamma p\rightarrow K^+\Sigma^0$	$d\sigma$	*	–	**	–	–	*	–	*	***	–
$\gamma p\rightarrow K^+\Sigma^0$	$\sigma_{\rm tot}$	*	*	**	**	*	**	*	**	***	****
$ep\rightarrow e'K^+\Sigma^0$	$d\sigma_{UL}$	**	*	–	*	–	–	–	**	*	–
$K^-p\rightarrow\gamma\Sigma^0$	Branching ratio	–	–	–	****	–	–	–	–	–	–
$\gamma p\rightarrow K^0\Sigma^+$	$\sigma_{\rm tot}$	****	****	–	–	–	–	–	****	****	****

vidual effects, seem undesirable.

The three Δ resonances ($D3$, $D4$, and $D7$), forbidden in the $K\Lambda$ reactions, play non-negligible roles in all neutral and charged Σ production processes.

In summary, within the several thousands of configurations studied, the SL model comes out to be the *simplest* and offers the best agreement with the data.

Finally, we emphasize that the extracted values for the two main coupling constants $g_{K\Lambda N}$ and $g_{K\Sigma N}$ (Tables VIII and IX) coming from $K\Lambda$ and $K\Sigma$ channels agree with each other within the associated uncertainties. The other couplings for these channels cannot be compared to each other, since they are products of the electromagnetic and the strong vertices.

IV. RESULTS AND DISCUSSION

In this section, we present our results for all the channels (1.1)–(1.7) and compare them with the data and relevant models from AS [2], WJC [3,28], and MBH [14]. Notice that for these models, the numerical results reported here have been obtained by using our code for reaction mechanisms (including coupling constants) as reported in the original papers. We will discuss, in appropriate subsections, eventual deviations from the curves given in those papers. We will also produce predictions for single- and double-photoproduction polarization asymmetries for observables (Table IV) to be measured soon at CEBAF, ELSA, and ESRF. These models allow, of course, extracting the two other sets of double-polarization asymmetries; namely, beam-target and target-recoil observables. These observables are harder to measure, so to reduce the number of figures in this paper, we do not depict them here.

A. Reaction $\gamma+p\rightarrow K^++\Lambda$

Since the recent publication of the experimental results from ELSA [8], a rather large number of data points for K^+ photoproduction channels below 1.5 GeV are available. In the energy range from 1.5 to 2.1 GeV the data [10] are still scarce, and at higher energies there are basically no data up to 4 GeV. In this and the following subsections, we present results for a few kinematical regions selected with respect to the existing or expected data. Although the models, ours included, have been obtained by fitting data up to roughly 2.1 GeV, we will report on some predictions up to 2.5 GeV, in order to investigate the higher energy behavior of different models. For the AS model the results are reported up to 1.5 GeV, the upper limit of its validity.

Figures 4(a)–(c), show the excitation functions for three c.m. angles of the produced kaons. Our model (SL) and that by WJC [3] reproduce the data at 27° almost equally well, while as expected, the AS model [2] overpredicts the data above 1.5 GeV. At the two other angles, SL gives the best agreement. It is also worthwhile mentioning that although the two first models (SL and WJC) give comparable results at the most forward angle in the whole energy range, they differ significantly in their predictions at the two other angles above 1.5 GeV, where no data are available. The angular distributions are given in Figs. 4(d)–(f) at three energies: close to threshold [Fig. 4(d)], at the highest limit for SL and WJC models [Fig. 4(f)], and at an intermediate energy [Fig. 4(e)], which is the upper limit for both the AS model and the recent data from ELSA. At 1.0 GeV [Fig. 4(d)], the data are too scattered and the models do not show significant differences, except for our model at most backward angles. At 1.45 GeV [Fig. 4(e)] our fit is again superior to the predictions of the two other models. The most striking feature appears at 2.1 GeV [Fig. 4(f)], where the two higher energy models reproduce the only fitted data point but give very different predictions in almost the whole angular range. The total cross section is depicted in Fig. 5. The existing data again rather favor our model (SL).

By now, it is well known [49,61] that polarization observables are much more sensitive to the model ingredients than the above observables. We first consider the single polarization asymmetries [Figs. 6(a)–(f)].

The most extensive polarization data concern the Λ-polarization asymmetry P[11], especially at 90° (Fig.

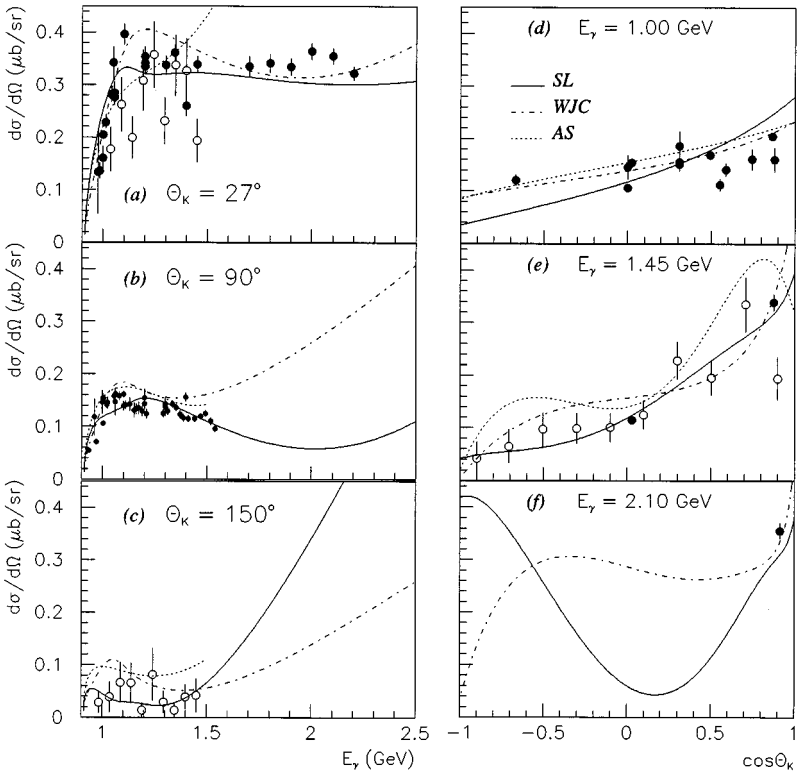

FIG. 4. Differential cross section for the process $\gamma p \to K^+\Lambda$: excitation functions at $\theta_K^{\rm cm}$ = 27° (a), 90° (b), and 150° (c), and angular distribution at $E_\gamma^{\rm lab}$ = 1.0 GeV (d), 1.45 GeV (e), and 2.1 GeV (f). The curves are from models SL (solid), WJC (dash-dotted), and AS (dotted). The AS curves are plotted up to the upper limit for this model, $E_\gamma^{\rm lab}$ = 1.5 GeV. Data are from Refs. [8] (empty circles), and [10] (solid circles).

6(a)]. At this angle, the fitted curves (the SL model and that by WJC), and the prediction by AS reproduce the data well enough. From the angular distribution at 1.45 GeV, Fig. 6(d), we infer that the backward angle measurements at intermediate energies are quite suitable in constraining phenomenological models. Results at other energies, not reported here, show that the highest sensitivity of the single-polarization asymmetries to the model ingredients is observed at energies around 1.5 GeV.

There are only three data points [12] with large error bars involving the polarized target asymmetry T, which fix at least the sign of this observable [2,66] in the relevant phase space. These data are well reproduced [Fig. 6(b)] by the present model (SL) and the prediction by AS. In contrast, the WJC model prediction gives the wrong sign. The angular distributions at intermediate energy [Fig. 6(e)] leads to the same conclusions as for the P asymmetry discussed above.

For linearly polarized photon beam no data are available, but measurements are foreseen at CEBAF and ESRF. Figures 6(c) and 6(f) show the predictions of different models and, compared to the two other single-polarization asymmetries, underline higher sensitivities to the reaction mechanisms put forward by these models.

The double-polarization measurements, using polarized beams and measuring the polarization of the outgoing hyperon, will constitute the first generation of the double-polarization experiments at ESRF and likely at CEBAF.

Figures 7(a)–(h) show predictions for the beam-recoil asymmetries. The observables $C_{x'}$ and $C_{z'}$ corresponding to a circularly polarized beam, show sizable sensitivities to the models in large areas of the phase space [Figs. 7(a) and (b) and 7(e) and (f)].

With a linearly polarized beam, the two asymmetries $O_{x'}$ and $O_{z'}$, Figs. 7(c) and (d) and 7(g) and (h), manifest less sensitivity to the reaction mechanism ingredients. The WJC model, contrary to the AS model, predicts rather tiny values for these observables almost through the whole phase space, while the present model gives intermediate values with sign changes at both energies. Such structures are discussed in the following.

Actually, in the polarization asymmetries shown in Figs. 6 and 7, a large number of curves, in particular those from the present model, undergo sign changes because of vanishing values (nodes) of the investigated observables. The physical content of these zero points (according to their positions and/or number) has been found [61,64] to be powerful ways to pin down the reaction mechanism. Hence, the polarization asymmetry measurements are expected to put drastic constraints to find a viable model.

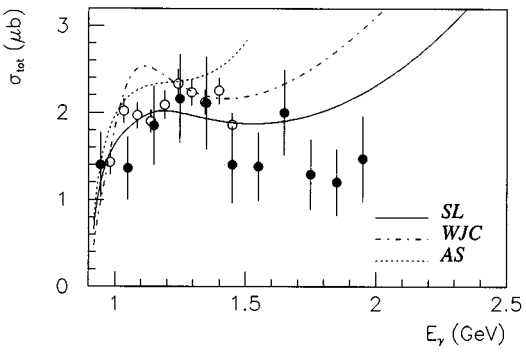

FIG. 5. Total cross section for the reaction $\gamma p \to K^+\Lambda$ as a function of photon energy. Curves and data as in Fig. 4.

B. Reaction $\gamma + p \to K^+ + \Sigma^0$

For this channel, the two most recent studies come from WJC [3] and MBH [14]. Only the latter authors were able to

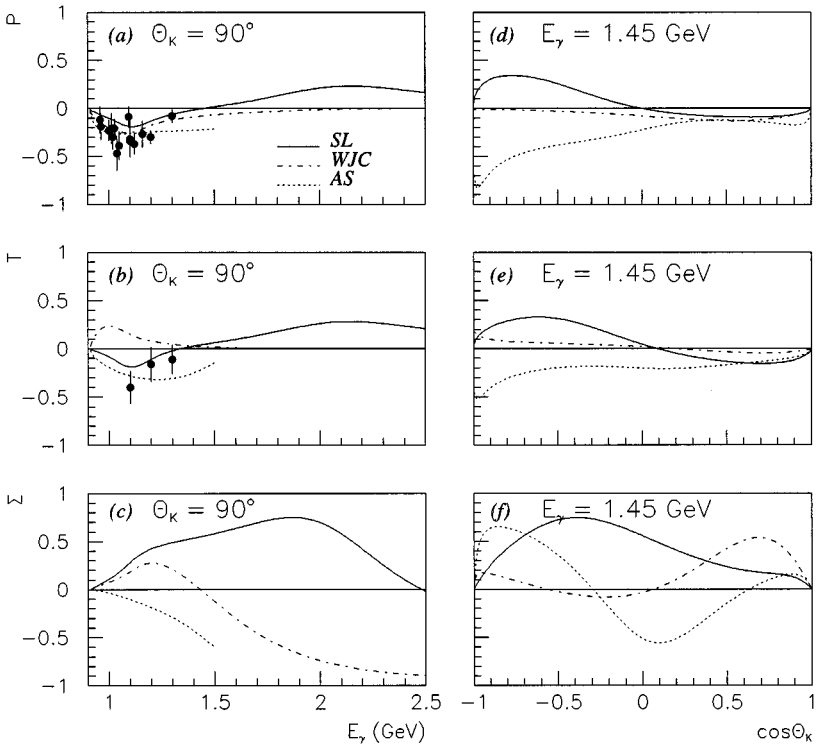

FIG. 6. Λ-polarization asymmetry (P) in $\gamma p \to K^+ \vec{\Lambda}$, polarized target asymmetry (T) in $\gamma \vec{p} \to K^+ \Lambda$, and linearly polarized beam asymmetry (Σ) in $\vec{\gamma} p \to K^+ \Lambda$: excitation functions at $\theta_K^{\rm cm} = 90°$ (a)–(c), and angular distributions at $E_\gamma^{\rm lab} = 1.45$ GeV (d)–(f). Curves are as in Fig. 4, and data from Refs. [11] (P) and [12] (T).

include the recent ELSA data [8] in their fitting procedures. We have also included the ELSA results in our data base. Figures 8(a)–(c) show the excitation functions at three angles of the produced kaons. Our model gives the best agreement with the data at all angles displayed. The results for the MBH model are satisfactory at the two extreme angles, but they deviate significantly from the data at 90°. We recall that the curves labeled WJC and MBH have been obtained using our code[7] with the relevant reaction mechanisms.

The angular distributions are given in Figs. 8(d)–(f) in a similar energy region as in the previous subsection [Figs. 4(d)–(f)]. At the lowest [1.1 GeV, Fig. 8(d)] and intermediate [1.45 GeV, Fig. 8(e)] energies, the three models give comparable agreement with the data. At the highest energy [2.1 GeV, Fig. 8(f)] they differ less drastically in their predictions, compared to the $K^+\Lambda$ channel case [Fig. 4(f)].

The total cross section (Fig. 9) is well described by the SL and WJC models, while the MBH curve exhibits a peculiar behavior at low energies, as is the case in Figs. 8(a) and (b). This latter model at energies above 2 GeV, predicts a flat behavior for the total cross section, while the two other models show a minimum below this energy.

For this reaction no polarization data are available.[8] We compare then the predictions of the three models among themselves in the same phase space region as for the previous reaction.

The outgoing baryon asymmetry (P) is depicted in Fig. 10. The excitation function at 90° [Fig. 10(a)], and the angular distribution at 1.45 GeV [Fig. 10(d)], show the most drastic differences basically between the MBH model on one hand, and the SL and WJC models on the other hand. All three models predict rather small asymmetries at higher energies.

For the polarized target asymmetry (T), the predictions of our model are significantly different from those of the two other ones for both the excitation function at 90° [Fig. 10(b)] and the angular distribution at 1.45 GeV [Fig. 10(e)].

As for the previous reaction, the polarized beam asymmetry (Σ) offers the most contrasted predictions from different

[7]Notice that our code closely reproduces the results published by MBH for both this reaction and the $K^0\Sigma^+$ channel discussed in the next subsection. However, the WJC curves, as reported here, compared to those released by the authors [3,28] require some comments. Our code reproduces all numerical results reported in [3,28] for both processes $\gamma + p \to K^+ + \Lambda$ and $\gamma + p \to K^+ + \Sigma^0$, except for the excitation function of the latter reaction at 27°. In trying to understand the origin of this discrepancy, we did several tests using both our code, and the code for the $\gamma + p \to K^+ + \Sigma^0$ channel kindly made available to us by Dr. R. A. Williams. We checked the agreement between numerical results from the Williams code and ours especially by producing excitation functions reported in [3,28] at 27°, 45°, and 90°. The two codes agree at the level of a few percent. At the most forward angle, both codes give the WJC curve as shown in Fig. 8(a), which hence deviates from that of Ref. [3], especially at higher energies. We did not pursue further the origins of the only difference for the $K^+\Sigma^0$ excitation function at 27° between the two codes and the corresponding curve in Ref. [3]. A possible explanation may be in the values used for mass/width of the Δ resonances, present only in the $K^+\Sigma^0$ channel. Using consistent mass/width values published in 1992 (Ref. [53]) and 1994 (Ref. [54]) by the Particle Data Group, we checked that such differences affect more the forward angle cross sections.

[8]The recent integrated polarization data from ELSA [8] have been reported in energy and/or angular bins too large to be embodied in minimization procedures. Hence, we do not consider that data here.

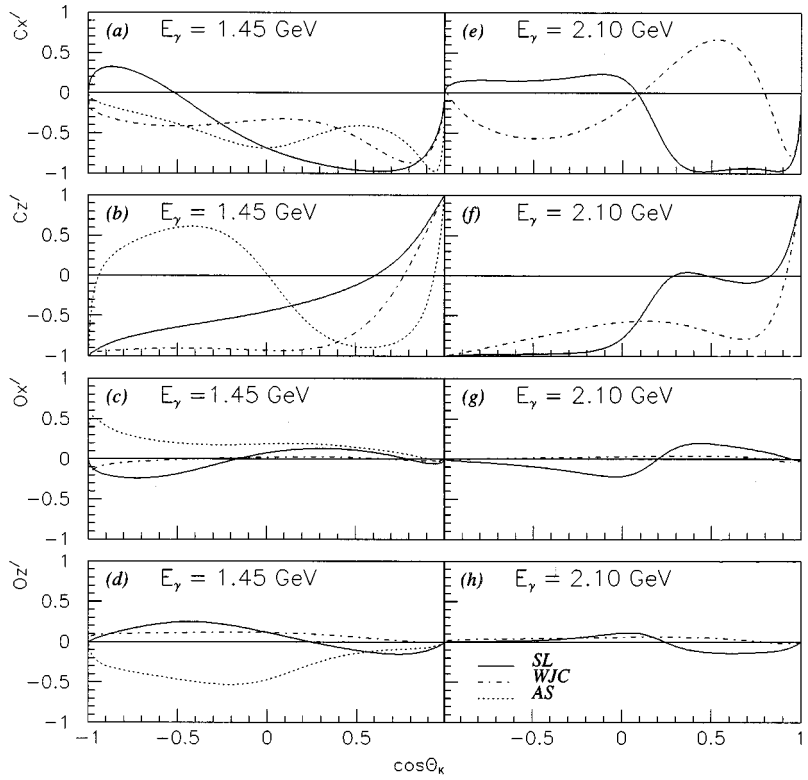

FIG. 7. Angular distributions for double polarization asymmetries ($C_{x'}$, $C_{z'}$, $O_{x'}$, and $O_{z'}$) in $\vec{\gamma}p \to K^+\vec{\Lambda}$ at $E_\gamma^{\rm lab} = 1.45$ GeV (a)–(d) and 2.1 GeV (e)–(h); curves as in Fig. 4.

models. This is clear for the excitation function at 90° [Fig. 10(c)] above 1.5 GeV. At 1.45 GeV [Fig. 10(f)] WJC gives predictions for angular distribution with opposite sign to those of the two other models in almost the whole angular range.

For the double-polarization observables with circularly polarized photon beams ($C_{x'}$ and $C_{z'}$), quite striking differences are observed between the present model and those by WJC and MBH. The $C_{x'}$ asymmetry at intermediate energy [Fig. 11(a)] seems to offer the most attractive phase space region. This is also the case for the $C_{z'}$ asymmetry [Fig. 11(b)].

The common feature to the three models for the two other double-polarization observables considered here with lin-

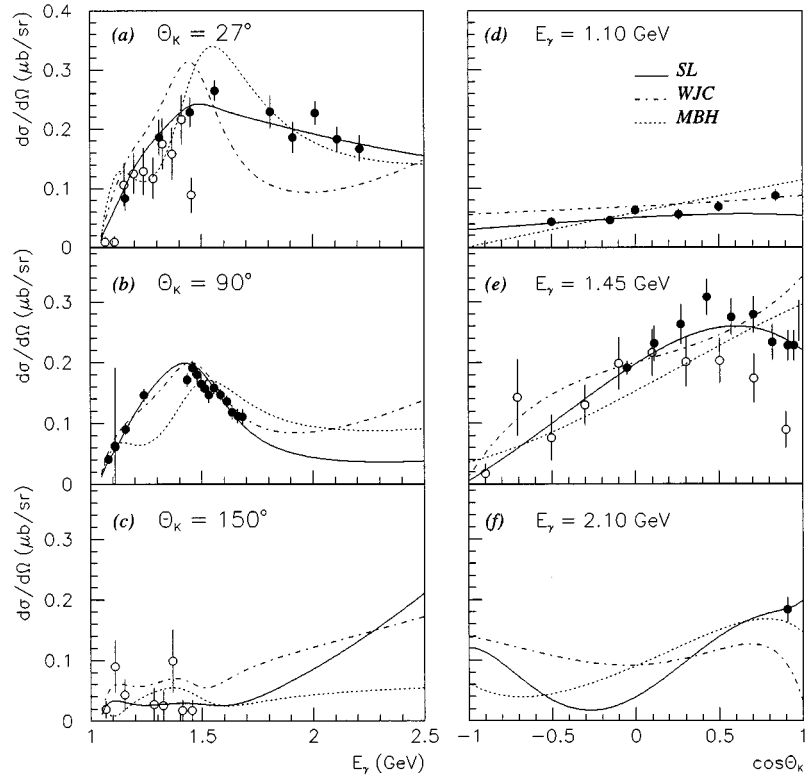

FIG. 8. Differential cross section for the process $\gamma p \to K^+\Sigma^0$: excitation functions at $\theta_K^{\rm cm} = 27°$ (a), 90° (b), and 150° (c), and angular distribution at $E_\gamma^{\rm lab} = 1.1$ GeV (d), 1.45 GeV (e), and 2.1 GeV (f). The curves are from models SL (solid), WJC (dash-dotted), and MBH (dotted). Data are from Refs. [8] (empty circles), and [10] (solid circles).

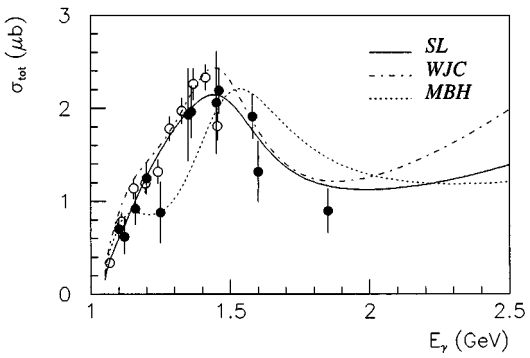

FIG. 9. Total cross section for the reaction $\gamma p \to K^+\Sigma^0$ as a function of photon energy. Curves and data as in Fig. 8.

early polarized photon beams ($O_{x'}$ and $O_{z'}$), is that they have smaller magnitudes than the two observables discussed above. For $O_{x'}$ [Figs. 11(c) and 11(g)], our model shows significant differences with the two other models at both energies. For $O_{z'}$, the angular distributions at 1.45 GeV [Fig. 11(d)] and 2.1 GeV [Fig. 11(h)] indicate smaller discrepancies between the SL and the two other models.

C. Reaction $\gamma + p \to K^0 + \Sigma^+$

For this channel, there are only two total cross section data points [15]. Only very recently, this reaction has been investigated through phenomenological approaches [14,57,58]. In this section, we show the results of the models SL and MBH [14], respectively, as well as the predictions for the relevant observables with the WJC [3] reaction mechanism.

The total cross section results of the three models and the data are depicted in Fig. 12(a). The prediction by the WJC model overestimates the two data points by roughly factors of 5 and 25 at the lowest and the highest energies, respectively. Compared with WJC, the fit by MBH improves the agreement with the data at the highest energy only, reducing the discrepancy between theory and experiment to roughly a factor of 10. Clearly, our model gives much better agreement with the data.

Given the existing proposals at CEBAF and ESRF, we show in Fig. 12 the predictions of the above models for the excitation function at 90° [Fig. 12(b)] and angular distributions at 1.5 GeV [Fig. 12(c)], and 2.1 GeV [Fig. 12(d)]. Except at lower energies at 90°, the SL and MBH models obtained by fitting the data, show important differences in their predictions. This emphasizes the crucial constraints that experimental results for this channel will put on the phenomenological investigations.

D. Reactions $e + p \to e' + K^+ + Y; Y \equiv \Lambda, \Sigma^0$

The electroproduction data [16] are even more scarce than in the case of photoproduction processes and have been obtained in a rather small phase space region. Among the new facilities, only CEBAF offers excellent conditions for forthcoming data [7].

Figure 13 shows the unpolarized component of the differential cross section $d\sigma_{UL} = d\sigma_U + \varepsilon_L d\sigma_L$ [see Eq. (2.24)],

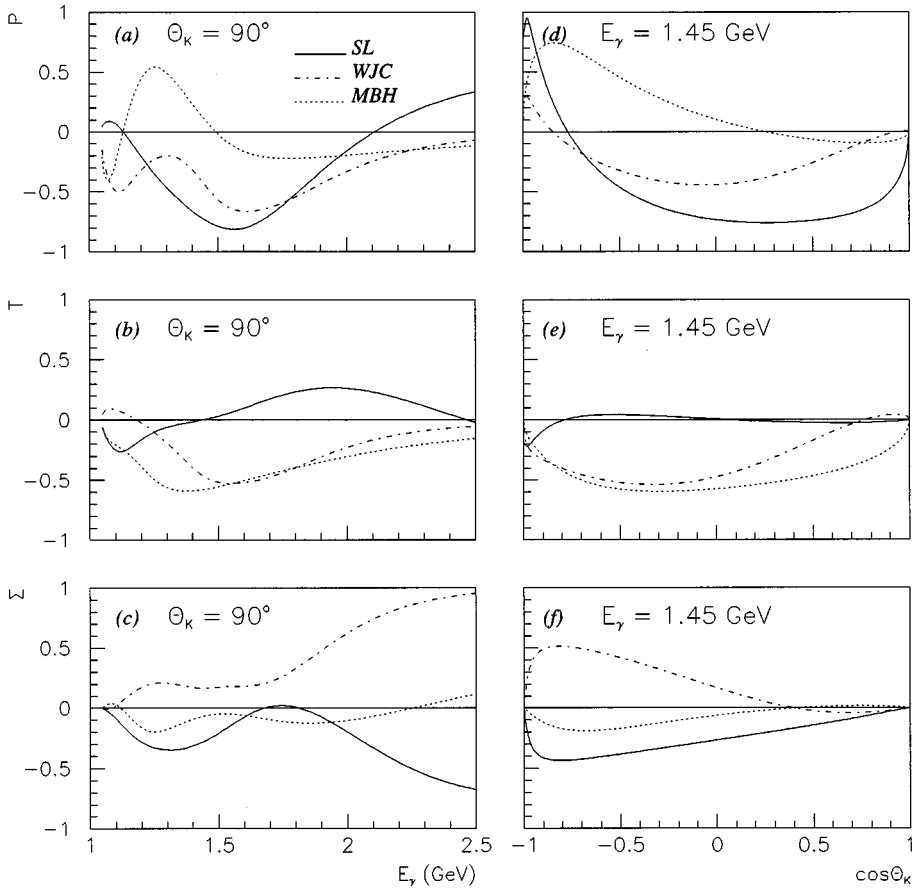

FIG. 10. Σ^0-polarization asymmetry (P) in $\gamma p \to K^+\vec{\Sigma}^0$, polarized target asymmetry (T) in $\gamma \vec{p} \to K^+\Sigma^0$, and linearly polarized beam asymmetry (Σ) in $\vec{\gamma} p \to K^+\Sigma^0$: excitation functions at $\theta_K^{cm} = 90°$ (a)–(c), and angular distributions at $E_\gamma^{lab} = 1.45$ GeV (d)–(f). Curves as in Fig. 8.

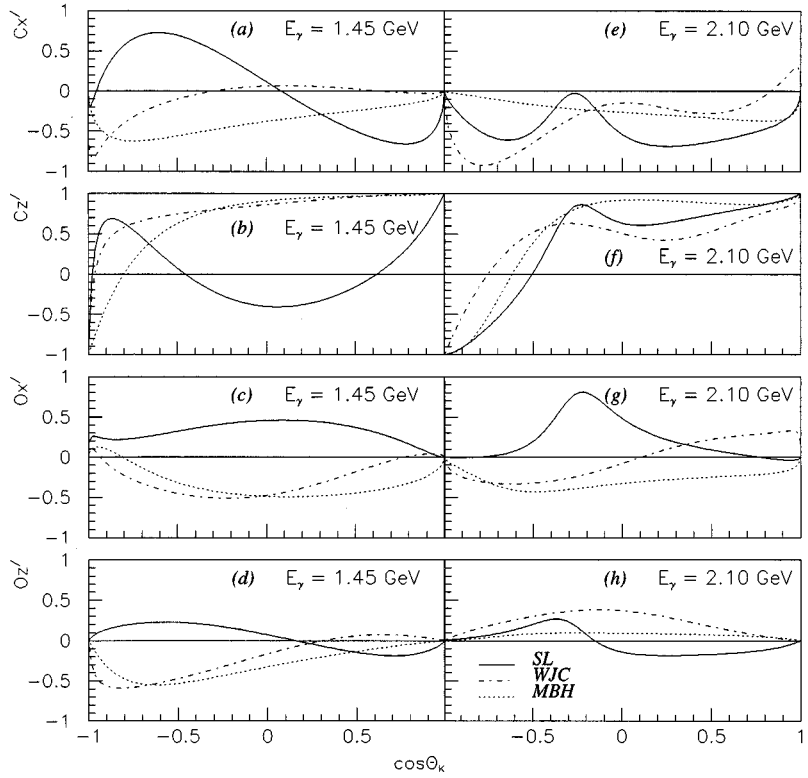

FIG. 11. Excitation function for double-polarization asymmetries ($C_{x'}$, $C_{z'}$, $O_{x'}$, and $O_{z'}$) in $\vec{\gamma}p \to K^+\vec{\Sigma}^0$ at $E_\gamma^{\rm lab} = 1.45$ GeV (a)–(d) and 2.1 GeV (e)–(h). Curves as in Fig. 8.

as a function of the transfer momentum for the reactions $e+p \to e'+K^+ +\Lambda$ and $e+p \to e'+K^+ +\Sigma^0$. The SL model reproduces well enough the data for both channels. This is also the case for the WJC model [3].

One of the major issues in the strangeness electroproduction concerns the information that can be extracted on the form factors of the relevant hadrons. We have performed a rather extensive study on this question. To get the highest

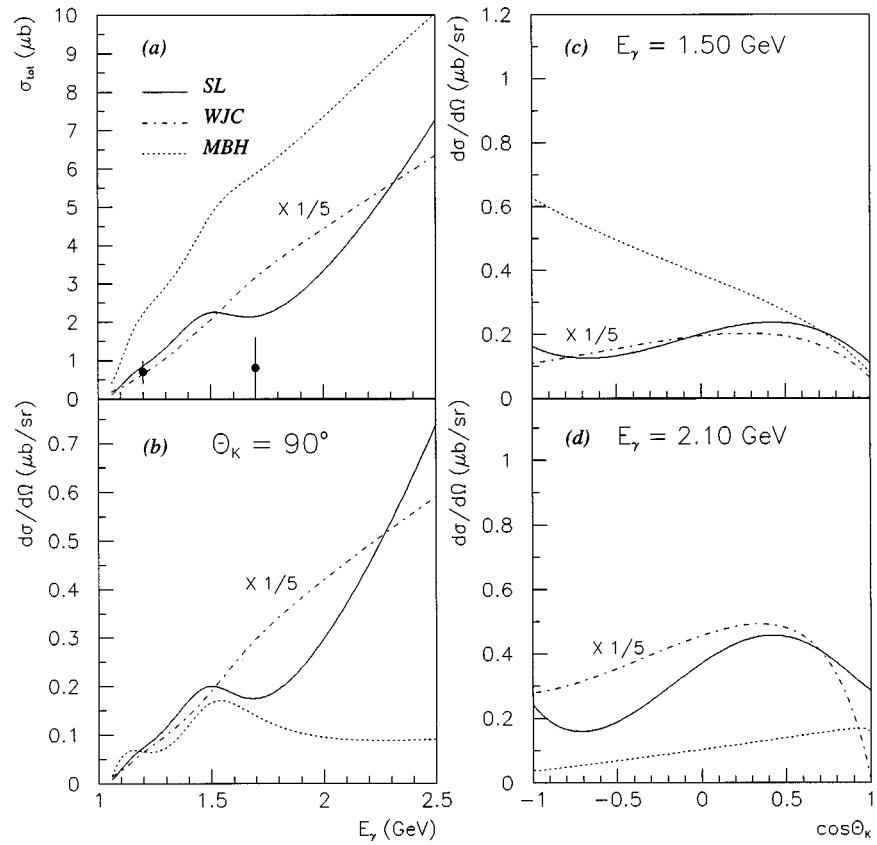

FIG. 12. Observables for the reaction $\gamma p \to K^0\Sigma^+$: total cross section as a function of photon energy (a), excitation function at $\theta_K^{\rm cm} = 90°$ (b), and angular distributions at $E_\gamma^{\rm lab} = 1.5$ GeV (c), and 2.1 GeV (d). Curves as in Fig. 8. The results for the WJC model are divided by a factor of 5. Data are from Ref. [15].

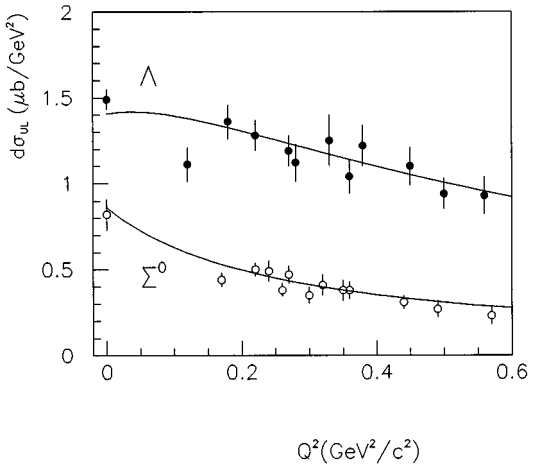

FIG. 13. Differential cross section $d\sigma_{UL}=d\sigma_U+\varepsilon_L d\sigma_L$ as a function of momentum transfer (Q^2) for the reactions $ep\to e'K^+\Lambda$ and $ep\to e'K^+\Sigma^0$, at $\varepsilon=0.72$, $s=5.02$ GeV^2, $t=-0.15$ GeV ^{2}. Curves are from the SL model, and data from Ref. [16].

sensitivity to the treatment of the hadronic structures, we have focused on the $K^+\Lambda$ channel, which has simpler reaction mechanism than the $K^+\Sigma^0$ reaction.

Figure 14 shows our results for $d\sigma_{UL}$ for different combinations of the form factors. As discussed in Sec. II C, we have chosen the baryons form factors by Gari and Krümpelmann published in 1985 (Ref. [38]) and 1992 (Ref. [39]), hereafter referred to as GK85 and GK92, respectively. For the t-channel exchanged particles, namely, K, K^*, and $K1$, the expressions by Adelseck-Wright [17], Williams *et al.* [3,28], and Cardarelli *et al.* [41] are used, and will be hereafter referred to as *A*, *W*, and *C* respectively. To facilitate the discussion, we will characterize each curve in Figs. 14–16 as *U-VXY*, where *U* refers to the choice of the baryons form factors, and *V*, *X*, and *Y* to those of the kaon, K^*, and $K1$, respectively. With this convention, the SL model corresponds to the combination GK92-WAA [curve (a) in Fig. 14]. The sensitivity of this observable to the kaon form factor is studied by using the alternative expression Eq. (2.20) based on Cardarelli *et al.* [41] work, which leads to curve (b) in Fig. 14 corresponding to GK92-CAA. For this configuration, as well as for each of the subsequent ones [curves (c)–(e)], we have fitted the data with the *same* exchanged particles as SL and extracted a *new* set of coupling constants to calculate the observables. In the SL model, we use the Adelseck-Wright [17] form factors (Sec. II C 2) for both $K1$ and K^* resonances. [9] Curves (c) and (d) show the results obtained if using the form factors as parametrized by Williams *et al.* [3,28], corresponding hence to the combinations GK92-WAW and GK92-WWW, respectively. Finally, in the latter case we have replaced the baryons form factors in SL (GK92) by the older version of the work published by Gari and Krümpelmann in 1985 (Ref. [38]). This configuration, GK85-WWW, is almost[10] the same as that used by Williams *et al.* [3,28] for the form factors.

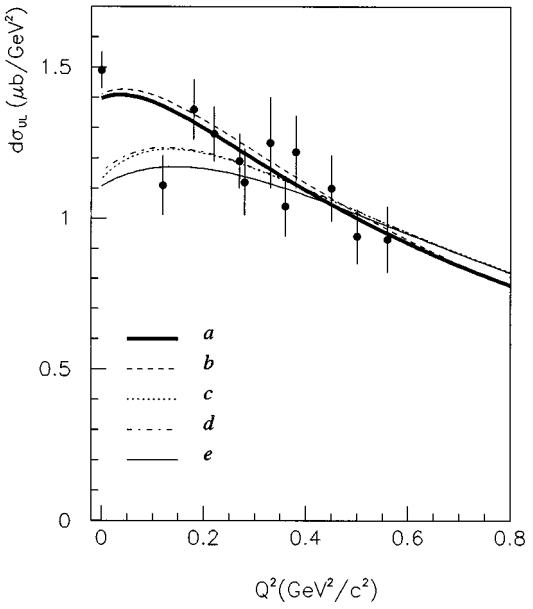

FIG. 14. Same as Fig. 13, but only for the reaction $ep\to e'K^+\Lambda$. Curves are from the SL model with the following combinations for electromagnetic form factors of the relevant hadrons (as defined in Sec. IV D): GK92-WAA (*a*), -CAA (*b*), -WAW (*c*), -WWW (*d*), and GK85-WWW (*e*).

Figure 14 shows that the unpolarized cross section $d\sigma_{UL}$ is not significantly sensitive to the different kaon form factors studied here [curves (a) and (b)]. This might be due to the fact that the form factors are constrained by the available data (although limited to small transfers), which is not the case for the kaonic resonances. The other three sets of form factors for $K1$, K^*, and baryons [curves (c)–(e)] show rather small and comparable deviations from the SL model only at low momentum transfer. Within this study, the unpolarized cross section does not show appealing features with respect to the hadrons form factors.

Now, we use the same five combinations of the form factors as above to investigate the sensitivity of different components of the differential cross section in Eq. (2.24) as a function of the Mandelstam variable t; namely, the transverse $d\sigma_U$, longitudinal $d\sigma_L$, transverse-longitudinal $d\sigma_I$, and longitudinal-longitudinal $d\sigma_P$ terms, depicted in Fig. 15.

The transverse cross section $d\sigma_U$ shows an almost uniformly decreasing behavior as a function of t, except for the (e) configuration. The phase space shows unequal sensitivities to the choice of the form factors. This latter observation is true also for the longitudinal part $d\sigma_L$, where the predictions bear more different behaviors as in the case of the transverse component. The interference terms, as expected, are smaller in magnitude than the unpolarized components. Although the transverse-longitudinal part ($d\sigma_I$) shows higher discrepancies between different sets of form factors than the transverse-transverse cross section ($d\sigma_P$), they stay compatible with the indications inferred from the existing

[9]These form factors allow obtaining a better fit to the data than those by WJC. This probably comes from the fact that the free parameters of the monopole form factors were fitted on an electroproduction data base close enough to the one considered here. For a comparison among different parametrizations, see Refs. [43,60].

[10]The only difference is that Williams *et al.* put $F_1^n(Q^2)=0$.

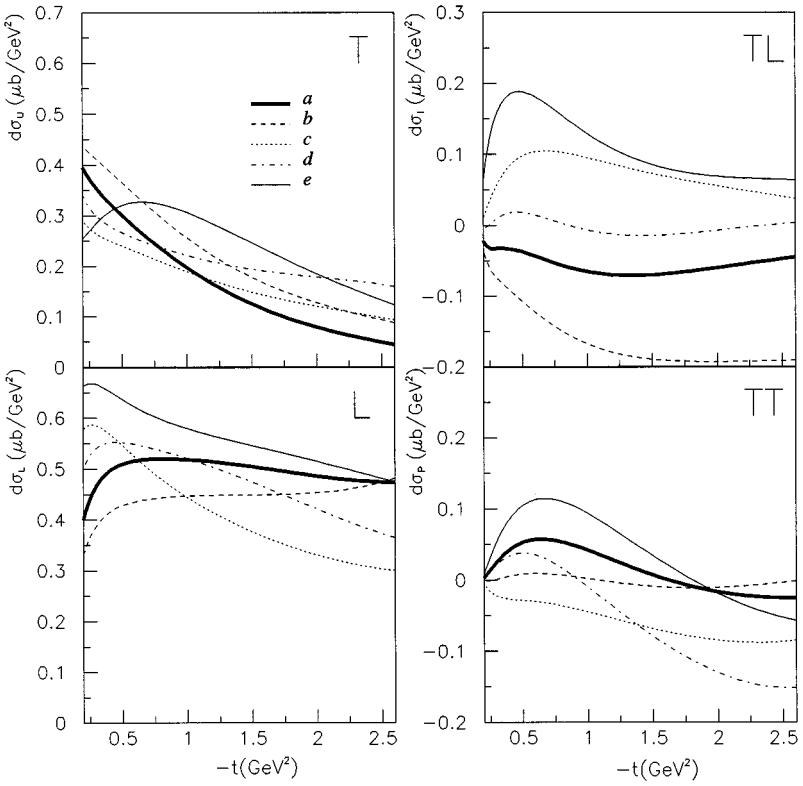

FIG. 15. Same as Fig. 14, but for the differential cross sections $d\sigma_U(t)$, $d\sigma_L(t)$, $d\sigma_I(t)$, and $d\sigma_P(t)$, and $\varepsilon=0.72$, $Q^2=1$ GeV^2. T and L stand for transverse and longitudinal, respectively.

very poor experimental data [16].

The sensitivity of the $K^+\Lambda$ electroproduction observables to the choice of the form factors is magnified for the ratio of the longitudinal to transverse cross sections $R(t)=d\sigma_L/d\sigma_U$ (Fig. 16). The SL model has a continuously increasing dependence on the $-t$ variable and gives above roughly $-t=1$ GeV^2 the highest ratio [notice that in Fig. 16 curve (a) is rescaled by a factor of 1/2]. The main effect when using the kaon form factor by Cardarelli *et al.* [41] is to reduce the magnitude of the ratio by almost a factor of 2 [curve (b)]. This form factor corresponds to the case where the radius (mass) of the *s* quark is different from those of *u* and *d* quarks. The crude approximation taking the same radius (mass) for all three quarks leads [43] to significantly smaller ratio and flattens its t dependence. A drastic change both in the shape and magnitude is produced by the use of WJC form factor for the $K1$ resonance [curve (c)]. The main sensitivity to the K^* form factor happens at the highest values of $-t$: above roughly 1.5 GeV^2, the ratio decreases slowly [curve (d)]. The other drastic effect is obtained by using the older version [38] of the baryonic form factors due to Gari and Krümpelmann, with the most striking feature being the inversion of the curvature at low values of $-t$ [curve (e)]. As mentioned above, the (e) configuration for the form factors is very close to that used by Williams *et al.* Actually, their model, although with a reaction mechanism very different from the present work (Table VIII), shows comparable behavior for $R(t)$. Moreover, the curvature of this ratio was found very sensitive to the t-channel contributions [60]. Such indications are very instructive, since we might hope that the forthcoming experimental data, in fixing the shape of this ratio, will offer a good opportunity to disentangle the role played by the hadrons form factors from those of the underlying reaction mechanism.

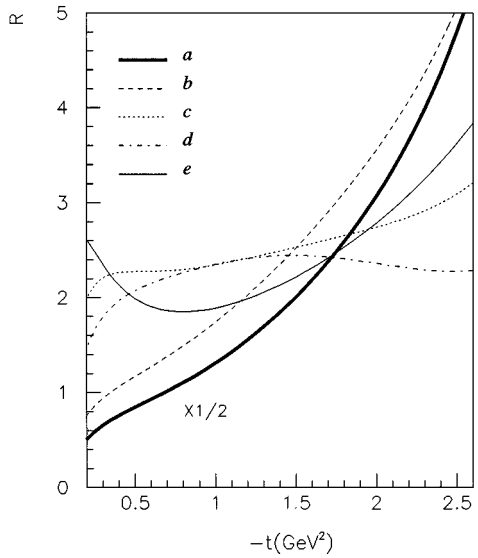

FIG. 16. Same as Fig. 14, but for the longitudinal to transverse differential cross sections ratio $R(t)=d\sigma_L/d\sigma_U$. Results for curve (a) are divided by a factor of 2.

To summarize the form factors studies, according to our results, the most significant information is embedded in the ratio $R(t)=d\sigma_L/d\sigma_U$ in the transfer range accessible at CEBAF.

E. Reactions $K^-+p\rightarrow\gamma+Y$; $Y\equiv\Lambda,\Sigma^0$

The radiative capture reactions have been mainly studied [67] independently of the photoproduction reactions and in

TABLE XII. Branching ratios from WJC [3], SS [69], and the present work (SL). Data are from Ref. [20].

	WJC	SS	SL	Experiment
$K^-p\to\gamma\Lambda$	0.89	1.09	0.95	0.86 ± 0.07 ± 0.09
$K^-p\to\gamma\Sigma^0$	1.46	1.55	1.43	1.44 ± 0.12 ± 0.11

tight connection with the role and the nature of the $\Lambda(1405)$ resonance. The field has suffered from the fact that the only data point [68] available until 1989, and used extensively in phenomenological calculations, was found to be too high by almost a factor of 3 compared to the new and more reliable measurements [20]. The most recent investigation in this sector has been done by Siegel and Saghai [69] (hereafter called SS), where all elastic and inelastic channels (hadronic and electromagnetic final states) in low energy K^-p interactions have been investigated within a coupled channel formalism. The authors discuss different results according to the allowed discrepancies for the coupling constants from their SU(3)-symmetry values. Here we report their results with 20% SU(3) breaking, as is the case in the present work.

The simultaneous study of these channels and the strangeness photoproduction reactions, using crossing symmetry, was basically initiated by Williams-Ji-Cotanch [3] after the new data became available. Table XII summarizes the results from SS, WJC, this work, and the experimental values. The data are well reproduced by the three models. Our calculations confirm the crucial role played by the $\Lambda(1405)$ resonance in this channel (see Table XI). New data from DAΦNE [70] will hopefully allow improving our understanding of this field.

V. SUMMARY AND CONCLUSIONS

The present work, based on an isobaric formalism, offers a unified description of all the strangeness photo- and electroproduction observables off the proton known experimentally in the energy range from threshold to $E_\gamma^{\rm lab}\simeq 2.1$ GeV; namely, $\gamma p\to K^+\Lambda$, $K^+\Sigma^0$, $K^0\Sigma^+$, and $ep\to e'K^+\Lambda$, $e'K^+\Sigma^0$, as well as the branching ratios of the radiative capture reactions $K^-p\to\gamma\Lambda,\gamma\Sigma^0$ at threshold, *via* crossing symmetry.

This formalism is an extension of previous calculations, the main novelty being the inclusion of spin-3/2 and -5/2 nucleonic resonances. We have used the method proposed by Adelseck *et al.* [25] for spin-3/2, and extended it to the spin-5/2 case. Nevertheless, adopting this treatment may be considered as an *ad hoc* method aimed to preserve gauge invariance of the amplitudes. Due to the effective Lagrangian theory [33], it is known that the treatment of an interacting spin-3/2 baryon implies the off-shell behavior of the particle (or resonance) at the vertex. This problem has recently been renewed by Benmerrouche *et al.* [34], and applied [35,36] to the nonstrange pseudoscalar mesons photoproduction. Our preliminary results [37] for kaon photoproduction show rather moderate effects due to the off-shell contributions.

The work presented in this paper leads to a reaction mechanism including, besides the extended Born terms, the exchange of the following particles:[11]

$$K^*(892),K1(1270),$$

$$N(1440)[1(1/2^+)],N(1720)[1(3/2^+)],N(1675)[2(5/2^-)],$$

$$\Lambda(1405)[0(1/2^-)],\Lambda(1670)[0(1/2^-)],\Lambda(1810)[1(1/2^+)],$$

$$\Sigma(1660)[1(1/2^+)],$$

$$\Delta(1910)[1(1/2^+)],\Delta(1232)[1(3/2^+)],\Delta(1920)[1(3/2^+)].$$

The three Δ resonances intervene only in the $K\Sigma$ channels. This set of exchanged resonances was determined after examining thousands of configurations containing different combinations of roughly 30 baryonic resonances. The obtained model is the only configuration satisfying the criteria specified in the text; namely, acceptable χ^2's for all the seven channels, agreement with the SU(3)-symmetry constraints for the two main coupling constants, predictivity power, and a rather simple reaction mechanism.

The free parameters of the model, 15 for the $K^+\Lambda$ and 20 for the $K\Sigma$ channels, have been determined by least-squares fitting procedure on 309 and 241 data points, respectively, for the above seven reactions, i.e., all the processes for which data are available.

In fact, the obtained model, called SL, contains a reasonable number of resonances, with the values of the two main coupling constants in agreement with the SU(3)-symmetry constraints. The model allows predicting the only unfitted available data for the target asymmetry polarization in the $\gamma\vec{p}\to K^+\Lambda$ reaction. These data were excluded purposely from the fitted data base to check the predictive power of the model. Given the planned photoproduction polarization experiments at CEBAF, ELSA, and ESRF, we provide predictions and go through a rather detailed discussion on the selectivity of single and double beam-recoil polarization observables in determining the reaction mechanism.

The present investigation emphasizes the need for new and more accurate data for all the strangeness production observables, and singles out the crucial need for measurements with polarized photon beams. The most appealing observables come out to be the single-polarization asymmetry using a (linearly) polarized beam, and the double-polarization observables with circularly polarized photons. The neutral kaon production channel $\gamma p\to K^0\Sigma^+$ appears also to be very attractive in pinning down the reaction mechanism.

In studying the electroproduction reactions, we emphasize the sensitivity of differential cross sections to the choice of baryonic and kaonic form factors as reported in the literature. We find that the most appropriate quantity to be measured is the ratio of the longitudinal to transverse components $R(t)=d\sigma_L/d\sigma_U$ as a function of the Mandelstam variable t.

[11]The quantum numbers of the baryons are indicated as $[l_{KY}(J^\pi)]$.

The radiative capture branching ratios at rest show, as expected, high sensitivity to the $\Lambda(1405)$ hyperonic resonance. We observe also a non-negligible role played by the $\Lambda(1670)$ resonance.

The elementary operators constructed here, because of the Lorentz invariant structure of the used formalism, can easily be transformed into any reference frame. These operators can, hence, be incorporated into strangeness production on nuclei, and especially in the promising field of the hypernuclear physics using electromagnetic probes.

ACKNOWLEDGMENTS

We are grateful to F. Tabakin for his careful reading of the manuscript. It is a pleasure to thank R. Adelseck, C. Bennhold, P. Bosted, Ch. Charles, G. Chanfray, R. Frascaria, M. Gari, M. Guidal, D. Menze, T. Mizutani, F. Piron, G. Salmè, R. A. Schumacher, P. Siegel, S. Simula, and R. A. Williams for several stimulating discussions and helpful exchanges. One of us (J.C.D.) would like to thank Commissariat à l'Energie Atomique for a pleasant and fruitful stay at the Service de Physique Nucléaire (DSM/DAPNIA) as post doc.

APPENDIX A

Contributions to the invariant amplitudes arising from the Born terms, and from the exchange of the K^*, the nucleonic $J^\pi = 1^\pm/2$, and the hyperonic $J^\pi = 1^\pm/2$ resonances.

1. Born terms $[(Y,Y')\equiv(\Lambda,\Sigma^0),(\Sigma^0,\Lambda)]$

$$\mathcal{A}_1^{\rm Born}=\frac{eg_{KYN}}{s-M_p^2}(F_1^p+\kappa_p F_2^p)+\frac{eg_{KYN}}{u-M_Y^2}(F_1^Y+\kappa_Y F_2^Y)+\frac{eg_{KY'N}}{u-M_{Y'}^2}\frac{(M_{Y'}+M_Y)\kappa_{\Sigma^0\Lambda}}{2M_p}F_2^{Y'},$$

$$\mathcal{A}_2^{\rm Born}=\frac{eg_{KYN}}{(s-M_p^2)(t-M_K^2)}\left[(F^K+F_1^p)+(F^K-F_1^p)\frac{p_\gamma\cdot p_K+p_\gamma\cdot p_p}{p_\gamma\cdot p_Y}\right],$$

$$\mathcal{A}_3^{\rm Born}=\frac{eg_{KYN}}{s-M_p^2}\frac{\kappa_p}{M_p}F_2^p,$$

$$\mathcal{A}_4^{\rm Born}=\frac{eg_{KYN}}{u-M_Y^2}\frac{\kappa_Y}{M_Y}F_2^Y+\frac{eg_{KY'N}}{u-M_{Y'}^2}\frac{\kappa_{\Sigma^0\Lambda}}{M_p}F_2^{Y'},$$

$$\mathcal{A}_5^{\rm Born}=\frac{eg_{KYN}}{s-M_p^2}\frac{\kappa_p}{2M_p}F_2^p-\frac{eg_{KYN}}{u-M_Y^2}\frac{\kappa_Y}{2M_Y}F_2^Y-\frac{eg_{KY'N}}{u-M_{Y'}^2}\frac{\kappa_{\Sigma^0\Lambda}}{2M_p}F_2^{Y'},$$

$$\mathcal{A}_6^{\rm Born}=\frac{-2\,eg_{KYN}}{(s-M_p^2)(t-M_K^2)}\left[F^K+(F^K-F_1^p)(p_\gamma^2-2p_\gamma\cdot p_K)\times\frac{p_\gamma\cdot p_p}{p_\gamma^2 p_\gamma\cdot p_Y}\right]+\frac{eg_{KYN}}{u-M_Y^2}\frac{2F_1^Y}{p_\gamma^2}.$$

2. Born terms ($Y\equiv\Sigma^+$)

$$\mathcal{A}_1^{\rm Born}=\frac{eg_{KYN}}{s-M_p^2}(1+\kappa_p)+\frac{eg_{KYN}}{u-M_Y^2}(1+\kappa_Y),$$

$$\mathcal{A}_2^{\rm Born}=\frac{-2\,eg_{KYN}}{(s-M_p^2)(u-M_Y^2)},$$

$$\mathcal{A}_3^{\rm Born}=\frac{eg_{KYN}}{s-M_p^2}\frac{\kappa_p}{M_p},$$

$$\mathcal{A}_4^{\rm Born}=\frac{eg_{KYN}}{u-M_Y^2}\frac{\kappa_Y}{M_Y},$$

$$\mathcal{A}_5^{\rm Born}=\mathcal{A}_6^{\rm Born}=0.$$

In the following $Y\equiv\Lambda,\Sigma^0,\Sigma^+$.

3. K^* resonance

$$\mathcal{A}_1^{K^*}=\frac{G_V}{M}\frac{M_Y+M_p}{t-M_{K^*}^2+iM_{K^*}\Gamma_{K^*}}F^{K^*}+\frac{G_T}{M}\frac{t}{M_Y+M_p}\frac{1}{t-M_{K^*}^2+iM_{K^*}\Gamma_{K^*}}F^{K^*},$$

$$\mathcal{A}_2^{K^*}=\frac{G_T}{M}\frac{1}{M_Y+M_p}\frac{1}{t-M_{K^*}^2+iM_{K^*}\Gamma_{K^*}}F^{K^*},$$

$$\mathcal{A}_3^{K^*}=\frac{G_V}{M}\frac{1}{t-M_{K^*}^2+iM_{K^*}\Gamma_{K^*}}F^{K^*}-\frac{G_T}{M}\frac{M_Y-M_p}{M_Y+M_p}\frac{1}{t-M_{K^*}^2+iM_{K^*}\Gamma_{K^*}}F^{K^*},$$

$$\mathcal{A}_4^{K^*}=\frac{G_V}{M}\frac{1}{t-M_{K^*}^2+iM_{K^*}\Gamma_{K^*}}F^{K^*}+\frac{G_T}{M}\frac{M_Y-M_p}{M_Y+M_p}\frac{1}{t-M_{K^*}^2+iM_{K^*}\Gamma_{K^*}}F^{K^*},$$

$$\mathcal{A}_5^{K^*}=\mathcal{A}_6^{K^*}=0.$$

4. $K1$ resonance

$$\mathcal{A}_1^{K1}=\mathcal{A}_5^{K1}=\mathcal{A}_6^{K1}=0,$$

$$\mathcal{A}_2^{K1}=-\frac{G_T^{K1}}{M}\frac{1}{M_Y+M_p}\frac{1}{t-M_{K1}^2+iM_{K1}\Gamma_{K1}}F^{K1},$$

$$\mathcal{A}_3^{K1}=\frac{G_V^{K1}}{M}\frac{1}{t-M_{K1}^2+iM_{K1}\Gamma_{K1}}F^{K1}+\frac{G_T^{K1}}{M}\frac{M_Y-M_p}{M_Y+M_p}\frac{1}{t-M_{K1}^2+iM_{K1}\Gamma_{K1}}F^{K1},$$

$$\mathcal{A}_4^{K1}=-\frac{G_V^{K1}}{M}\frac{1}{t-M_{K1}^2+iM_{K1}\Gamma_{K1}}F^{K1}-\frac{G_T^{K1}}{M}\frac{M_Y-M_p}{M_Y+M_p}\frac{1}{t-M_{K1}^2+iM_{K1}\Gamma_{K1}}F^{K1}.$$

In the above expressions, we use $M=1$ GeV as a renormalization mass.

5. $N^*(1/2^{\pm})$ nucleonic resonances

$$\mathcal{A}_2^{N^*(1/2^{\pm})}=\mathcal{A}_4^{N^*(1/2^{\pm})}=\mathcal{A}_6^{N^*(1/2^{\pm})}=0,$$

$$\mathcal{A}_1^{N^*(1/2^{\pm})}=\frac{eg_{KYN^*}}{s-M_{N^*}^2+iM_{N^*}\Gamma_{N^*}}\times\frac{(M_{N^*}+M_p)\kappa_{N^*N}}{2M_p}\frac{M_{N^*}-M_p}{M_{N^*}\mp M_p}F^{N^*},$$

$$\mathcal{A}_3^{N^*(1/2^{\pm})}=\pm\frac{eg_{KYN^*}}{s-M_{N^*}^2+iM_{N^*}\Gamma_{N^*}}\frac{\kappa_{N^*N}}{M_p}F^{N^*},$$

$$\mathcal{A}_5^{N^*(1/2^{\pm})}=\pm\frac{eg_{KYN^*}}{s-M_{N^*}^2+iM_{N^*}\Gamma_{N^*}}\frac{\kappa_{N^*N}}{2M_p}F^{N^*}.$$

The contributions from the s-channel $\Delta^*(1/2^{\pm})$ resonances associated with Σ^0 production have the same form, with the appropriate substitutions for the mass, width and coupling constant.

6. $Y^*(1/2^{\pm})$ hyperonic resonances

$$\mathcal{A}_2^{Y^*(1/2^{\pm})}=\mathcal{A}_3^{Y^*(1/2^{\pm})}=\mathcal{A}_6^{Y^*(1/2^{\pm})}=0,$$

$$\mathcal{A}_1^{Y^*(1/2^{\pm})}=\frac{eg_{KNY^*}}{u-M_{Y^*}^2+iM_{Y^*}\Gamma_{Y^*}}\times\frac{(M_{Y^*}+M_Y)\kappa_{Y^*Y}}{2M_p}\frac{M_{Y^*}-M_Y}{M_{Y^*}\mp M_Y}F^{Y^*},$$

$$\mathcal{A}_4^{Y^*(1/2^{\pm})}=\pm\frac{eg_{KNY^*}}{u-M_{Y^*}^2+iM_{Y^*}\Gamma_{Y^*}}\frac{\kappa_{Y^*Y}}{M_p}F^{Y^*},$$

$$\mathcal{A}_5^{Y^*(1/2^{\pm})}=\mp\frac{eg_{KNY^*}}{u-M_{Y^*}^2+iM_{Y^*}\Gamma_{Y^*}}\frac{\kappa_{Y^*Y}}{2M_p}F^{Y^*}.$$

APPENDIX B

After simplifications and factorizations with the help of MAPLE, the contributions to the invariant amplitudes corresponding to the exchange of an $N^*(3/2^+)$ resonance are the following.

The photoproduction amplitudes are written as

$$\mathcal{A}_j=\frac{1}{(s-M_{N^*}^2+iM_{N^*}\Gamma_{N^*})}\sum_{i=1}^{2}G_iP_{ij},\quad j=1,\ldots,4.$$

The contributions coming from the G_1 coupling are

$$P_{11}=\frac{(3\sqrt{s}-M_p)A}{6s}+M_\Lambda-\frac{p_\Lambda\cdot p_\gamma}{\sqrt{s}+M_p},\quad P_{12}=-\frac{1}{\sqrt{s}+M_p},$$

$$P_{13}=\frac{M_\Lambda}{\sqrt{s}+M_p}-\frac{M_pA}{3s(\sqrt{s}+M_p)},\quad P_{14}=1,$$

and those coming from the G_2 coupling

$$P_{21}=-\frac{B(\sqrt{s}-M_p)}{6\sqrt{s}(\sqrt{s}+M_p)},\quad P_{22}=\frac{\sqrt{s}-M_p}{2(\sqrt{s}+M_p)^2},$$

$$P_{23}=\frac{p_\Lambda\cdot p_\gamma}{(\sqrt{s}+M_p)^2}-\frac{B(\sqrt{s}-M_p)}{3(\sqrt{s}+M_p)^2\sqrt{s}},$$

$$P_{24}=-\frac{\sqrt{s}-M_p}{2(\sqrt{s}+M_p)},$$

with

$$A=2p_\Lambda\cdot q-\sqrt{s}M_\Lambda,\quad B=p_\Lambda\cdot q+\sqrt{s}M_\Lambda.$$

The electroproduction amplitudes are

$$\mathcal{A}_j=\frac{1}{(s-M_{N^*}^2+iM_{N^*}\Gamma_{N^*})}\sum_{i=1}^{2}G_iE_{ij},\quad j=1,\ldots,6.$$

For $j=1,\ldots,4$, the E_{ij} coefficients are expressed in terms of the above P_{ij} as

$$E_{ij}=P_{ij}+p_\gamma^2R_{ij},\quad i=1,2,\quad j=1,\ldots,4.$$

The extra terms R_{ij} coming from the G_1 coupling have the following expressions:

$$R_{11}=\frac{A}{6s(\sqrt{s}+M_p)},\quad R_{12}=\frac{A}{6s(\sqrt{s}+M_p)p_\Lambda\cdot p_\gamma},$$

$$R_{13}=0,\quad R_{14}=0,$$

and those coming from G_2

$$R_{21}=\frac{B}{6(\sqrt{s}+M_p)^2\sqrt{s}},$$

$$R_{22}=-\frac{\sqrt{s}M_\Lambda M_p-2M_pp_\Lambda\cdot q+3\sqrt{s}p_\Lambda\cdot q}{6p_\Lambda\cdot p_\gamma(\sqrt{s}+M_p)^2s},$$

$$R_{23}=-\frac{A}{3(\sqrt{s}+M_p)^2s},\quad R_{24}=\frac{1}{2(\sqrt{s}+M_p)^2}.$$

For $j=5,6$ the E_{ij} coefficients coming from G_1 and G_2 are

$$E_{15}=-\frac{A}{3s},\quad E_{16}=\frac{p_\gamma\cdot p_p A}{3s(\sqrt{s}+M_p)p_\Lambda\cdot p_\gamma}+\frac{1}{\sqrt{s}+M_p},$$

$$E_{25}=\frac{p_\gamma\cdot p_p A}{3(\sqrt{s}+M_p)^2 s},$$

$$E_{26}=-\frac{p_\gamma\cdot p_p(\sqrt{s}M_\Lambda M_p-2M_p p_\Lambda\cdot q+3\sqrt{s}p_\Lambda\cdot q)}{3p_\Lambda\cdot p_\gamma(\sqrt{s}+M_p)^2 s}.$$

In the above expressions, the dot products $p_\gamma\cdot p_p$, $p_\Lambda\cdot p_\gamma$ and $p_\Lambda\cdot q$ can be written in terms of the usual invariants as

$$p_\gamma\cdot p_p=\tfrac{1}{2}(s-p_\gamma^2-M_p^2),\quad p_\Lambda\cdot p_\gamma=\tfrac{1}{2}(M_\Lambda^2+p_\gamma^2-u),$$

$$p_\Lambda\cdot q=\tfrac{1}{2}(s+M_\Lambda^2-M_K^2).$$

In the case of a negative parity resonance, the $V^\nu(N^*p\gamma)$ vertex is given by Eq. (2.3) with $M_p\to -M_p$ and $i\gamma^5\to\mathbf{1}$, and the $V^\mu(K^+\Lambda N^*)$ vertex is obtained from Eq. (2.7) times $i\gamma^5$ (see Table II). The corresponding M_{fi} amplitude has the same structure as Eq. (2.6), with γ^5 acting now onto the right of the first vertex. Using the anticommutation property of γ^5 with γ^μ, it is easy to move the γ^5 matrix in the same position as in the positive parity case, namely onto the right of the second vertex. By inspection, we immediately obtain the parity rule for the transition matrix

$$M_{fi}^{(-)}=-M_{fi}^{(+)}[\sqrt{s}\to-\sqrt{s}].$$

The corresponding parity rule for the contributions to the invariant amplitudes is then

$$\mathcal{A}_j^{(-)}=-\mathcal{A}_j^{(+)}[\sqrt{s}\to-\sqrt{s}].$$

APPENDIX C

The contributions to the invariant amplitudes corresponding to the exchange of a $N^*(5/2^+)$ resonance have the same structure as in the spin-3/2 case. We give only the photoproduction amplitudes

$$\mathcal{A}_j=\frac{1}{10(s-M_{N^*}^2+iM_{N^*}\Gamma_{N^*})}\sum_{i=1}^{2}G_i P_{ij},\quad j=1,\ldots,4.$$

Defining $w=\sqrt{s}$, the contributions coming from the G_1 coupling are

$$P_{11}=\frac{\{(2M_\Lambda w(2w-M_p)p_\Lambda\cdot q-2(4w+M_p)(p_\Lambda\cdot q)^2)w_+-M_\Lambda^2 w^2 w_+^2\}w_-^2}{2w_-w^4}$$
$$+\frac{\{4w^2(7w+4M_p)p_\Lambda\cdot p_\gamma p_\Lambda\cdot q-4M_\Lambda w^3(2w-M_p)p_\Lambda\cdot p_\gamma\}w_--20(p_\Lambda\cdot p_\gamma)^2w^4}{2w_-w^4},$$

$$P_{12}=\frac{(4p_\Lambda\cdot q+M_\Lambda w)w_+w_--10p_\Lambda\cdot p_\gamma w^2}{w^2w_-},$$

$$P_{13}=\frac{\{2(p_\Lambda\cdot q)^2M_p-2M_\Lambda w(2w-M_p)p_\Lambda\cdot q\}w_+w_--M_\Lambda^2w^2w_+w_-^2-8w^2p_\Lambda\cdot p_\gamma M_p p_\Lambda\cdot q}{w_-w^4}+\frac{2M_\Lambda w^3(5w-M_p)p_\Lambda\cdot p_\gamma}{w_-w^4},$$

$$P_{14}=\frac{2w_+(3w-2M_p)p_\Lambda\cdot q-10p_\Lambda\cdot p_\gamma w^2-M_\Lambda w w_+^2}{w^2},$$

and those coming from G_2:

$$P_{21}=\frac{\{(p_\Lambda\cdot q)^2-M_\Lambda w p_\Lambda\cdot q\}w_+^2w_-+(2M_\Lambda w^3p_\Lambda\cdot p_\gamma-2p_\Lambda\cdot p_\gamma w^2p_\Lambda\cdot q)w_+}{2w_-w^3},$$

$$P_{22}=\frac{(-4p_\Lambda\cdot q-M_\Lambda w)w_+^2w_-+10w^2w_+p_\Lambda\cdot p_\gamma}{2w^2w_-^2},$$

$$P_{23}=\frac{\{M_\Lambda w p_\Lambda\cdot q-(p_\Lambda\cdot q)^2\}w_+^2w_-+\{4w(2w-M_p)p_\Lambda\cdot p_\gamma p_\Lambda\cdot q-M_\Lambda w^2(3w+M_p)p_\Lambda\cdot p_\gamma\}w_+}{w^3w_-^2}-\frac{10(p_\Lambda\cdot p_\gamma)^2w^3}{w^3w_-^2},$$

$$P_{24}=\frac{10w^2w_+p_\Lambda\cdot p_\gamma-2(3w-2M_p)w_+^2p_\Lambda\cdot q+M_\Lambda w w_+^3}{2w^2w_-},$$

with

$$w_+ = w + M_p, \quad w_- = w - M_p.$$

The dot products and the parity rule are expressed as in Appendix B.

APPENDIX D

The relations between the CGLN amplitudes and the $\mathcal{A}_j$ invariant functions are

$$\mathcal{F}_1 = (\sqrt{s} - M_p)\mathcal{A}_1 - p_\gamma \cdot p_p \mathcal{A}_3 - p_\gamma \cdot p_Y \mathcal{A}_4 - p_\gamma^2 \mathcal{A}_5,$$

$$\mathcal{F}_2 = \frac{|\boldsymbol{p}_\gamma||\boldsymbol{p}_K|}{(E_p + M_p)(E_Y + M_Y)}[(\sqrt{s} + M_p)\mathcal{A}_1 + p_\gamma \cdot p_p \mathcal{A}_3 + p_\gamma \cdot p_Y \mathcal{A}_4 + p_\gamma^2 \mathcal{A}_5],$$

$$\mathcal{F}_3 = \frac{|\boldsymbol{p}_\gamma||\boldsymbol{p}_K|}{(E_p + M_p)}[-2p_\gamma \cdot p_p \mathcal{A}_2 + (\sqrt{s} + M_p)\mathcal{A}_4 + p_\gamma^2 \mathcal{A}_6],$$

$$\mathcal{F}_4 = \frac{|\boldsymbol{p}_K|^2}{(E_Y + M_Y)}[2p_\gamma \cdot p_p \mathcal{A}_2 + (\sqrt{s} - M_p)\mathcal{A}_4 - p_\gamma^2 \mathcal{A}_6],$$

$$\mathcal{F}_5 = \frac{|\boldsymbol{p}_\gamma|^2}{(E_p + M_p)}[-\mathcal{A}_1 + 2p_\gamma \cdot p_Y \mathcal{A}_2 + (\sqrt{s} + M_p)(\mathcal{A}_3 - \mathcal{A}_5) + p_\gamma \cdot p_Y \mathcal{A}_6],$$

$$\mathcal{F}_6 = \frac{|\boldsymbol{p}_\gamma||\boldsymbol{p}_K|}{(E_Y + M_Y)}\Big[-2p_\gamma \cdot p_Y \mathcal{A}_2 + (\sqrt{s} - M_p)\mathcal{A}_3 - p_\gamma \cdot p_Y \mathcal{A}_6 - \frac{1}{E_p + M_p}\{p_{\gamma 0}\mathcal{A}_1 + p_\gamma \cdot p_p \mathcal{A}_3 + p_\gamma \cdot p_Y \mathcal{A}_4 + p_{\gamma 0}(\sqrt{s} + M_p)\mathcal{A}_5\}\Big].$$

The expressions for the different components of the cross section [Eq. 2.24] in terms of the CGLN amplitudes are

$$d\sigma_U = \mathcal{A}[|\mathcal{F}_1|^2 + |\mathcal{F}_2|^2 + 2\mathrm{Re}(\mathcal{F}_1^* \mathcal{F}_2)\cos\theta + \tfrac{1}{2}\sin^2\theta\{|\mathcal{F}_3|^2 + |\mathcal{F}_4|^2 + 2\mathrm{Re}(\mathcal{F}_1^* \mathcal{F}_4 - \mathcal{F}_2^* \mathcal{F}_3 + \mathcal{F}_3^* \mathcal{F}_4 \cos\theta)\}],$$

$$d\sigma_L = \mathcal{A}[|\mathcal{F}_7|^2 + |\mathcal{F}_8|^2 + 2\mathrm{Re}(\mathcal{F}_7^* \mathcal{F}_8)\cos\theta],$$

$$d\sigma_P = \mathcal{A}[\tfrac{1}{2}|\mathcal{F}_3|^2 + \tfrac{1}{2}|\mathcal{F}_4|^2 + \mathrm{Re}(\mathcal{F}_1^* \mathcal{F}_4 - \mathcal{F}_2^* \mathcal{F}_3 + \mathcal{F}_3^* \mathcal{F}_4 \cos\theta)],$$

$$d\sigma_I = \mathcal{A}\mathrm{Re}[\mathcal{F}_7(-\mathcal{F}_2^* + \mathcal{F}_3^* + \mathcal{F}_4^* \cos\theta) + \mathcal{F}_8(\mathcal{F}_1^* + \mathcal{F}_3^* \cos\theta + \mathcal{F}_4^*)],$$

with

$$\mathcal{A} = \frac{|\boldsymbol{p}_K|}{2\sqrt{s}} \frac{(E_p + M_p)(E_Y + M_Y)}{s - M_p^2},$$

$$\mathcal{F}_7 = \mathcal{F}_1 + \mathcal{F}_3 \cos\theta + \mathcal{F}_5, \quad \mathcal{F}_8 = \mathcal{F}_4 \cos\theta + \mathcal{F}_6.$$

[1] See, e.g., C. B. Dover and D. J. Millener, in *Modern Topics in Electron Scattering*, edited by B. Frois and I. Sick (World Scientific, Singapore, 1991).

[2] R. A. Adelseck and B. Saghai, Phys. Rev. C **42**, 108 (1990).

[3] R. A. Williams, C. R. Ji, and S. R. Cotanch, Phys. Rev. C **46**, 1617 (1992).

[4] J. Cohen, Int. J. Mod. Phys. A **4**, 1 (1989).

[5] Zh. Li, Phys. Rev. C **52**, 1648 (1995).

[6] A. Kumar, Ph.D. thesis, Ohio University, 1994; A. Kumar and D. S. Onley, Ohio University report 1994; V. Keiner, ''A Spectator-Quark-Model for the photoproduction of Kaons,'' Bonn University Report hep-ph/9501342, 1995; D. Lu, R. H. Landau, and S. C. Phatak, Phys. Rev. C **52**, 1662 (1995).

[7] See, e.g., R. A. Schumacher, Nucl. Phys. **A585**, 63c (1995); B. A. Mecking, Prog. Part. Nucl. Phys. **34**, 53 (1995).

[8] M. Bockhorst *et al.*, Z. Phys. C **63**, 37 (1994).

[9] See, e.g., GRAAL Collaboration, Grenoble Anneau Accélérateur Laser, ESRF-Grenoble report, 1992.

[10] P. L. Donoho and R. L. Walker, Phys. Rev. **112**, 981 (1958); B. D. McDaniel *et al.*, *ibid.* **115**, 1039 (1959); H. M. Brody *et al.*, *ibid.* **119**, 1710 (1960); R. L. Anderson *et al.*, Phys. Rev. Lett. **9**, 131 (1962); H. Thom *et al.*, *ibid.* **11**, 434 (1963); C. W. Peck, Phys. Rev. **135**, 830 (1964); R.L. Anderson *et al.*, unpublished; S. Mori, Ph.D. thesis, Cornell University, 1966; H. Thom, Phys. Rev. **151**, 1322 (1966); D. E. Groom and J. H. Marshall, *ibid.* **159**, 1213 (1967); A. Bleckmann *et al.*, Z. Phys. **239**, 1 (1970); D. Decamp *et al.*, Orsay Report LAL 1236, 1970; Th. Fourneron, Thèse de Doctorat d'Etat, Université de Paris, 1971; H. Goeing *et al.*, Nucl. Phys. **B26**, 121 (1971); T. Fujii *et al.*, Phys. Rev. D **2**, 439 (1970); P. Feller *et al.*, Nucl. Phys. **B39**, 413 (1972); R. Erbe *et al.*, Phys. Rev. **188**, 2060 (1969).

[11] B. Borgia *et al.*, Nuovo Cimento **32**, 218 (1964); M. Grilli *et al.*, *ibid.* **38**, 1467 (1965); D. E. Groom and J. H. Marshall, Phys. Rev. **159**, 1213 (1967); R. Hass *et al.*, Nucl. Phys. **B137**, 261 (1978).

[12] K. H. Althoff *et al.*, Nucl. Phys. **B137**, 269 (1978).

[13] C. Bennhold and L. E. Wright, Phys. Rev. C **39**, 927 (1989); C. Bennhold, *ibid.* **43**, 775 (1991).

[14] T. Mart, C. Bennhold, and C. E. Hyde-Wright, Phys. Rev. C **51**, R1074 (1995).

[15] R. Erbe *et al.*, Phys. Rev. **188**, 2060 (1969).

[16] C. N. Brown *et al.*, Phys. Rev. Lett. **28**, 1086 (1972); T. Azemoon *et al.*, Nucl. Phys. **B95**, 77 (1975); C. J. Bebek *et al.*, Phys. Rev. D **15**, 594 (1977); **15**, 3082 (1977); P. Brauel *et al.*, Z. Phys. C **3**, 101 (1979).

[17] R. A. Adelseck and L. E. Wright, Phys. Rev. C **38**, 1965 (1988); R. Adelseck, Ph.D. thesis, Ohio University, 1988.

[18] S. R. Cotanch and S. S. Hsiao, Nucl. Phys. **A450**, 419c (1986); H. Bando, T. Motaba, and J. Zofka, in *Perspectives of Meson*

Science, edited by T. Yamazaki *et al.* (North Holland, Amsterdam, 1992); S. Shinmura, Prog. Theor. Phys. **92**, 571 (1994).
[19] C. R. Ji and S. R. Cotanch, Phys. Rev. C **38**, 2691 (1988).
[20] D. A. Whitehouse *et al.*, Phys. Rev. Lett. **63**, 1352 (1989).
[21] H. Thom, Phys. Rev. **151**, 1322 (1966).
[22] F. M. Renard and Y. Renard, Nucl. Phys. **B25**, 490 (1971).
[23] Y. Renard, Nucl. Phys. **B40**, 499 (1972).
[24] S. S. Hsiao and S. R. Cotanch, Phys. Rev. C **28**, 1668 (1983).
[25] R. A. Adelseck, C. Bennhold, and L. E. Wright, Phys. Rev. C **32**, 1681 (1985).
[26] R. A. Williams, C. R. Ji, and S. R. Cotanch, Phys. Rev. D **41**, 1449 (1990); Phys. Rev. C **43**, 452 (1991).
[27] R. A. Adelseck and B. Saghai, Phys. Rev. C **45**, 2030 (1992).
[28] R. A. Williams, Ph.D. thesis, North Carolina State University, Raleigh, 1993.
[29] S. Fubini, Y. Nambu, and V. Wataghin, Phys. Rev. **111**, 329 (1958).
[30] Y. Renard, Thèse de Doctorat d'Etat ès-Sciences Physiques, Université des Sciences et Techniques du Languedoc, 1971.
[31] H. Pilkuhn, *The Interactions of Hadrons* (North-Holland, Amsterdam, 1967).
[32] J. C. David, Thèse de Doctorat, Université Claude Bernard Lyon-1, LYCEN T 9438, 1994.
[33] S. Weinberg, Phys. Rev. **166**, 1568 (1968); R. D. Peccei, *ibid.* **181**, 1902 (1969).
[34] M. Benmerrouche, R. M. Davidson, and N. C. Mukhopadhay, Phys. Rev. C **39**, 2339 (1989).
[35] R. M. Davidson, N. C. Mukhopadhay, and R. S. Wittman, Phys. Rev. D **43**, 71 (1991).
[36] M. Benmerrouche, N. C. Mukhopadhay, and J. F. Zhang, Phys. Rev. D **51**, 3237 (1995).
[37] J. C. David, C. Fayard, G. H. Lamot, T. Mizutani, and B. Saghai, unpublished.
[38] M. F. Gari and W. Krümpelmann, Z. Phys. A **322**, 689 (1985); Phys. Lett. B **173**, 10 (1986).
[39] M. F. Gari and W. Krümpelmann, Phys. Rev. D **45**, 1817 (1992).
[40] E. B. Dally *et al.*, Phys. Rev. Lett. **45**, 232 (1980); S. R. Amendolia *et al.*, Phys. Lett. B **178**, 435 (1986).
[41] F. Cardarelli, I. L. Grach, I. M. Narodetskii, E. Pace, G. Salmé, and S. Simula, Phys. Rev. D **53**, 6682 (1996).
[42] F. Cardarelli, I. L. Grach, I. M. Narodetskii, E. Pace, G. Salmé, and S. Simula , Phys. Lett. B **332**, 3 (1994).
[43] J. C. David, C. Fayard, G. H. Lamot, and B. Saghai, Saclay Report DAPNIA-SPHN-95-53, 1995.
[44] G. F. Chew, M. Goldberger, F. E. Low, and Y. Nambu, Phys. Rev. **106**, 1345 (1957).
[45] R. L. Workman and H. W. Fearing, Phys. Rev. D **37**, 3117 (1988).
[46] J. de Swart, Rev. Mod. Phys. **35**, 916 (1963).
[47] A. D. Martin, Nucl. Phys. **B179**, 33 (1981); M. Bozoian, J. C. H. Doremalen, and H. J. Weber, Phys. Lett. **122B**, 138 (1983); J. Antolin, Phys. Rev. D **35**, 122 (1987); R. G. E. Timmermans, Th. A. Rijken, and J. J. de Swart, Phys. Lett. B **257**, 227 (1991); R. G. E. Timmermans, Ph.D. thesis, Katholieke Universiteit Nijmegen, 1991.
[48] B. Saghai, in the CEBAF 1992 Summer Workshop, edited by F. Gross and R. Holt, AIP Conf. Proc. No. 269 (AIP, New York, 1992).
[49] B. Saghai, in *Proceedings of the Sixth Workshop on Perspectives at Intermediate Energies*, Trieste, 1993, edited by S. Boffi, C. Ciofi degli Atti, and M. Giannini (World Scientific, Singapore, 1994).
[50] F. James and M. Roos, MINUIT, CERN Report D506, 1981.
[51] Particle Data Group, unpublished.
[52] Particle Data Group, Phys. Lett. B **239**, (1990).
[53] Particle Data Group, Phys. Rev. D **45** (1992).
[54] Particle Data Group, Phys. Rev. D **50**, 1173 (1994).
[55] B. Krusche *et al.*, Phys. Rev. Lett. **74**, 3736 (1995).
[56] J. C. David, C. Fayard, G. H. Lamot, and B. Saghai, in *Proceedings of the 14th International Few-Body Conference*, Williamsburg, 1994, edited by F. Gross, AIP Conf. Proc. No. 334 (AIP, New York, 1995).
[57] F. Piron, M. S. dissertation, Saclay, 1994.
[58] J. C. David, C. Fayard, G. H. Lamot, F. Piron, and B. Saghai, in *8th International Symposium on Polarization Phenomena in Nuclear Physics*, Bloomington, 1994, edited by E. J. Stephenson and S.E. Vigdor, AIP Conf. Proc. No. 339 (AIP, New York, 1995).
[59] Ch. Charles, M. S. dissertation, Saclay, 1995.
[60] Ch. Charles, J. C. David, C. Fayard, M. Guidal, G. H. Lamot, and B. Saghai, Few-Body Sys. Suppl. **8**, 452 (1995).
[61] B. Saghai and F. Tabakin, Phys. Rev. C **53**, 66 (1996).
[62] See, e.g., S. J. Lindenbaum, *Particle-Interaction Physics at High Energies* (Clarendon Press, Oxford, 1973), Chap. 13, p. 444.
[63] C. Schmid and J. K. Storrow, Nucl. Phys. **B29**, 219 (1971).
[64] C. G. Fasano, F. Tabakin, and B. Saghai, Phys. Rev. C **46**, 2438 (1992).
[65] B. Saghai and F. Tabakin (unpublished).
[66] R. L. Workman, Phys. Rev. C **40**, 2922 (1989).
[67] See, e.g., J. Lowe, Nuovo Cimento **102A**, 167 (1989), and references therein.
[68] J. Lowe *et al.*, Nucl. Phys. **B209**, 16 (1982).
[69] P. Siegel and B. Saghai, Phys. Rev. C **52**, 392 (1995).
[70] See, e.g., *Proceedings of the Workshop on Physics and Detectors for DAΦNE* , Frascati, Italy, 1991, edited by G. Pancheri (Servizio Documentazione dei Laboratori Nazionali di Frascati, Frascati, 1991); FINUDA Collaboration, ''A Detector for Nuclear Physics at DAΦNE,'' Frascati Report LNF-93/021, 1993.